Escola Politécnica da Universidade de São Paulo
POLI-USP/SP

Pedro Costa Braga

Chemical Vapor Deposition growth of 2D material for Electronic Applications

TCC em Engenharia de Materiais

Dissertation submitted to the Examining Board as partial requirement for the Materials Engineer by the Polytechnic School of the University of São Paulo under the supervision of Prof. Flávio Beneduce Neto.

SÃO PAULO
2021

Pedro Costa Braga

Chemical Vapor Phase Deposition growth of 2D material for Electronic Applications

This report has been judged in the context of the conclusion of Materials Science Engineering course to the student Pedro Costa Braga.

São Paulo, 24 de novembro de 2021

Approved: _____
Flávio Beneduce Neto
Professor da EPUSP

Approved: _____
Hercilio Gomes de Melo
Professor da EPUSP

Approved: _____
Augusto Camara Neiva
Professor at EPUSP

Acknowledgments

I would like to thank my family deeply for being so supportive in the last few years, a loving and caring family which gave me the best education possible, whose example shaped my caracter and determination which I carried along my journey. I am grateful to my parents, Gina Magaly Costa Braga and João Pedro Braga who have been loving and supportive of my decisions whereas this meant changing school, changing state or changing country. I also would like to thank my siblins Barbara Costa Braga and Lucas Costa Braga, if I came this far it is only because they have paved the way before me.

Furthermore I would like to thank my friends who helped me all along this journey, the ones I met in France where we created a nice small family environmet ,we have shared our lives and traveled together ,also to the ones I met before going to Europe which set my mind and spirit free, opened my mind to the complexity delicacies and pains of life. In special I would like to thank my Arthurs friends (either the little one and the big one), for years long of friendship and great company, Yu for the loving philosophical talks, Tiago for always being my science best friend, (p)Mateus for the great teenager histories, and many other loving and caring friends such as: Mateus, Davi, André, Gabriela, Cadu, Beneti, Thiago, Carioca, Bahia, Arthur, Sato, Joao, Caio, Otavio, Vini, Nix, Fernanda, Gabriel, Lais, Giulia, André, Rafa, Cyril, Yona, Corentin, Juline, Adrian, Arriel and many others.

I would like to thank the folowing people, Prof. Andras Kis for the internship opportunity, without whose help I would not been able to set foot in such a prestigious university, without his faith in my potential none of this would have been possible, Hyungoo and Guilherme for being my double supervisors, the first in material science and the latter in electronics - without their help my work would have been considerably harder. My academic supervisors Hubert and Flavio for bureaucratic help and friendliness. Also, thanks to Lanes group for its hospitality.

My special thanks to my home university Escola Politecnica da Universidade de São Paulo for giving me the oportunity of doing my double degree and all its academic formation it gave through the years I attended there, as well as to Grenoble INP for receiving me in this great life experience in Europe for 2 years and all its academic knowledge.

Abstract

This dissertation discusses the fabrication of a MoS_2 transistor from the CVD deposition process to the deposition of the metallic contacts, going through several material characterization techniques such as AFM, PL, EDX, SEM, Raman and transistor characterization methods such as the "Output" and "Transfer" curves. Part of the novelty of this work is the usage of a showerhead system for growth. In addition to the detailed description of the fabrication and characterization techniques used, this work also presents growth and electrical characterization results of MoS_2 monolayer as well as discussions of Excitons, general properties of MoS_2, CVD, Electronic and Material Characterisation.

Résumé

Cette thèse traite de la fabrication d'un transistor MoS_2 depuis le processus de dépôt CVD jusqu'au dépôt des contacts métalliques, en passant par plusieurs techniques de caractérisation des matériaux telles que AFM, PL, EDX, SEM, Raman et des méthodes de caractérisation des transistors telles que les courbes "Output" et "Transfer". Une partie de la nouveauté de ce travail est l'utilisation d'un système de "showerhead" pour la croissance. En plus de la description détaillée des techniques de fabrication et de caractérisation utilisées, ce travail présente également les résultats de la croissance et de la caractérisation électrique de la monocouche de MoS_2 ainsi que des discussions sur les excitons, les propriétés générales de MoS_2, le CVD, la caractérisation électronique et des matériaux.

Resumo

Esta dissertação discute a fabricação de um transistor MoS_2 desde o processo de deposição CVD até a deposição dos contatos metálicos, passando por diversas técnicas de caracterização de materiais como AFM, PL, EDX, SEM, Raman e métodos de caracterização de transistores como as curvas de "Saída" e "Transferência". Parte da novidade deste trabalho é a utilização de um sistema de "showerhead" para crescimento. Além da descrição detalhada das técnicas de fabricação e caracterização utilizadas, este trabalho também apresenta resultados de crescimento e caracterização elétrica de MoS_2 monocamada, assim como discussões sobre Excitons, propriedades gerais de MoS_2, CVD, Caracterização Eletrônica e Material.

Contents

Glossary

- TMDC = transition metal dichalcogenide
- LED = Light emitting diode
- EPFL = École Polytechinique de Lausanne
- Lanes = Laboratory of Nanoscale Electronics and Structures
- PL = Photo luminescence
- CVD = Chemical Vapor Deposition
- SOC = Spin Orbit Coupling
- VB = Valence Band
- CB = Conduction Band
- FET = Field Effect Transistor
- MOCVD = Metallorganic Chemical Vapor Deposition
- AFM = Atomic Force Microscope
- DFT = Density Functional Theory
- SEM = Scanning Electron Microscopy
- EDX = Energy Discursive X-ray Spectroscopy
- Direct Band Gap = A material in which only needs energy (by a photon) to excite it's electron to conduction band
- Indirect Band Gap = A material in which needs energy (by a photon) and momentum (by a phonon) to excite it's electron to the conduction band

List of Figures

List of Tables

1 Introduction

Transistors, LED's, photo diodes among many others electronic components are the fundamental building blocks of today's computers, smartphones and other electronic devices. With an ever increasing demand of miniaturization and improvement of those electronic components in order to obtain faster processing speed and lower power consumption - humanity is now approaching the intrinsic physical limits of those traditional silicon components.

One of the promising approaches toward the improvement of electrical devices are the two-dimensional materials like graphene and MoS_2, which are just one to three atoms thick (lesser than 0.7 nm [15]), showing great electric and heat conductivity, great mechanical strength and good flexibility compared to their silicon counterparts, aside from the fact that they are the absolute miniaturization of a possible electronic component. This comes as an important factor for transistors to suppress the short channel effects that appear due to reduction of the transistor size[16].

Another important property of two-dimensional materials is the large exciton binding energy and its stability. Normally, for semiconductor devices, the absorption of a photon with adequate energy promotes an electron (e^-) to the conduction band leaving behind a hole (h^+) from the valence band. This electron/hole pair is responsible for conduction of charges in a semiconductor device. In two-dimensional materials this electron/hole pair bounds together creating an electrically neutral quasi particle known as exciton.

Excitons can be generated optically, and decay radiatively, therefore naturally creating photonic input/output without any outside element. At the same time, they may be electrically controlled during their finite lifetime. This could combine the scalability of electronics collectively with the speed and power performance of photons in a unique tool [8].

All those advantages do not come with an important setback: growth of MoS_2 in an industrialized environment. In the past years there have been numerous reports [17] of MoS_2 mono layer growth using different methods, some being able to grow nanometer size grains, others in the micrometer, but, so far, there have been few reports of growth using an industrial scale machine such as those fabricated by Aixtron [18] which is company that produces industrial machines for CVD growth. One of the main objective of this thesis is therefore create a viable and a reproductivable route for MoS_2 mono layer growth.

1.1 Presentation on the different actors of the internship

École Polytechnique Fédérale de Lausanne (EPFL) is one of the most prestigious Universities in the world, ranking in 14th place at the QS-World Ranking. It is specialized in engineering and natural sciences and is part of the Swiss Federal Institutes of Technology Domain with ETH Zurich. In connection with research and teaching activities, EPFL operates a nuclear reactor CROCUS, a Tokamak Fusion reactor, a Blue Gene/Q Supercomputer and P3 bio-hazard facilities.

EPFL is located at the French speaking side of Switzerland and has about 20,000 students with more than 125 nationalities present on campus and 48% of the student population being of foreign nationals.

Laboratory of Nanoscale Electronics and Structures (LANES) is an EPFL Laboratory that covers a wide range of topics. Two dimension materials grow, study of fundamental properties and applications in electronic, excitonic, spintronic and optoelectronic devices. The group is constituted by 14 members which are supervised

by Prof. Andras Kis.

In recent years the group has made formidable progress in the field of 2D materials, with its most know achievements being published in renewed papers such as Single-layer MoS_2 transistors at Nature nanotechnology and Electronics and optoelectronics of two-dimensional transition metal dichalcogenides at Nature nanotechnology.

Figure 1: EPFL Campus

1.2 Objectives of the internship

The main objective of the project is to contribute to the development of a 2D material and device synthesis process with the broad goal of enabling the production of excitonic devices for a wide range of applications based on synthetic materials. Such an approach currently does not exist and is the main hurdle in increasing the efficiency of electrical signals or the conversion between optical and electrical signals.

This is done by assisting other group members in the development of a scalable growth process for making 2D semiconductors that can be integrated into excitonic devices fabrication and characterisation. In this sense the tasks related to this internship can be planned out as:

1. Growth of MoS_2 (specially focused in varying the flow parameter of carries gases, temperature test, and observing the importance of a clean reactor);
2. Characterization of grown material;
3. Fabrication of field effect transistor and
4. Electrical characterization of device.

1.3 Organization of the report

The planning of the report follows the organization of the work done during the internship, in the first section, it will discuss the theoretical background of this work presenting the **Physical properties and synthesis of** MoS_2. In the next section the **Methods** used will also be discussed, pointing out the **Characterization** techniques used and the tools use to **Fabricate field effect transistor**. Next the **Results** of **Growth** will be discussed, explaining the important information about the morphology of the crystals as well as optical properties, after it will discuss the **Electrical properties** of the device fabricated.

2 Physical properties and synthesis of MoS_2

MoS_2 is material that has been know for more than 50 years. It is a semiconductors in its bulk form, and is commonly used in the industry as a dry lubricant because of its low friction and robustness. However, similar to graphite, when reduced down to an atomic monolayer it reveals entirely new properties. Monolayers of MoS_2 can sustain current densities 50 times larger than copper and have stiffness comparable to stainless steel, while being only 0.65 nm thick [8]. Figure 2 schematizes the crystal structure of MoS_2.

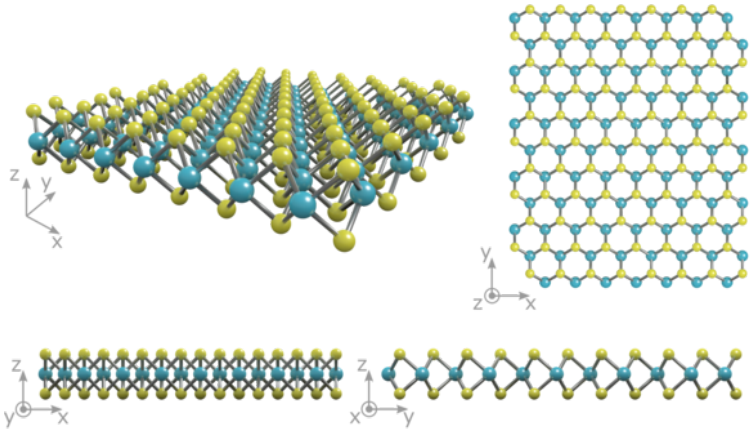

Figure 2: Atomic structure of monolayer MoS_2 [1].

2.1 Electronic Band Structure

The electronic band structure of a material dictates the possible energies that electrons may have whitin it, as well as forbidden energy levels. These properties are derived and calculated from quantum mechanical wave functions for a periodic lattice of atoms and are fundamental to understand many physical properties of solids such as optical absorption and applications in solid state devices such as transistors and solar cells.

This study can give important information about a MoS_2, such as the band gap, which is the energy difference between the valence band and the conduction band. Essentially, it represents the necessary energy that is required to promote an electron up to the conduction band where it can partake in the electric conduction. In a direct band gap the photon can be emitted without additional momentum change. In a "indirect" band gap, a photon cannot be emitted because the electron must have an additional momentum in order to transfer its energy to the crystal lattice and therefore decay. This property is fundamental for photonic devices because it greatly affects the radiative recombination of a given semi-conductor, with an indirect band-gap in order to the light be absorbed it must also involve the absorption or emission of a phonon, where the phonon momentum is greater or equal to the difference between the electron and hole momentum - this greatly reduces the radiative recombination of a given material. For this reason light-emitting devices such as diodes and lasers are mostly made out of direct band-gap materials.

One of the most remarkable properties of MoS_2 is the transition from an indirect band gap in its bulk form to direct band gap in monolayer form. Figure 3 shows the calculated band structure using Density Functional Theory (DFT) simulations of bulk form to monolayer limit. The reason for that is because the bandgap expands due to the quantum confinement out-of-plane direction, in a similarity with quantum dots [19].

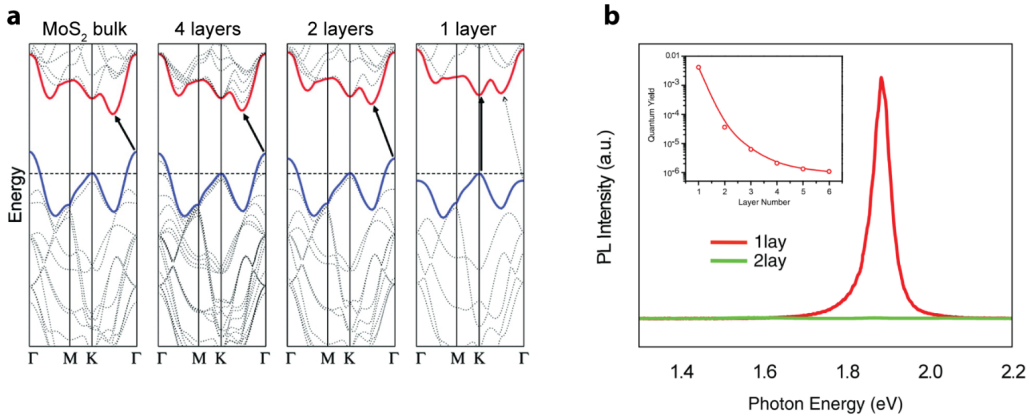

Figure 3: Calculated thickness-dependent band structures of MoS_2 . Indirect to direct bandgap transition occurs at the monolayer limit. (b) Photoluminescence observed from mono-(red) and bilayer (green) MoS_2 flakes. Inset shows PL quantum yield as a function of layer numbers. Figure from [2] [3].

2.2 Spin Orbit Coupling

The spin–orbit coupling is a relativistic type of interaction due to the particle's spin with its motion inside a potential. This interaction is mostly prominent in metal d orbitals such as those appeared in MoS_2, whereas in graphene is negligible.

In order to define the impact of spin-orbit coupling of MoS_2 it's relevant to determine it's Hamiltonian. From Figure 4 and according to D. Xiao et al in it's article: "Coupled spin and valley physics in monolayers of mos2and other group-vi dichalcogenides", it's possible to observe that the bulk form of MoS_2 has 2H stacking order with the space group D^4_{6H}, which is inversion symmetric. When it is in a monolayer form, the crystal symmetry reduces to D^1_{3H}, and inversion symmetry is explicitly broken: which means the Mo atom as the inversion center, S atom will be mapped onto an empty location. The two-band $k \cdot p$ Hamiltonian of MoS_2 close to the K point with spin-orbit coupling (SOC) has the form [8] [4]:

$$\hat{H}_0 = at(\tau k_x \hat{\sigma}_x + k_y \hat{\sigma}_y) + \frac{\Delta}{2}\hat{\sigma}_z - \lambda\tau\frac{\hat{\sigma}_z - 1}{2}\hat{s}_z \tag{1}$$

In which $\hat{\sigma}_{(x,y,z)}$ denotes the Pauli matrices for the two basis functions, a is the lattice constant, t the effective hopping integral, τ the valley index, Δ the energy gap, 2 is the spin splitting at the valence band top caused by the SOC and $\hat{s}_z$ is the Pauli matrix for spin [8] [4].

The values for the spin splitting in the valence band for MoS_2 is $\Delta VB \approx 150meV$, for the conduction band the splitting is two order of magnitude smaller $\Delta CB \approx 3meV$ [8] [4]. Spin-orbit coupling not only interfere in the direct-indirect band gap transition in MoS_2 but also poses odd parity under time reversal, opposite signs of band splitting are dictated by the time-reversal relation between K and -K valleys. This effect is better discussed in Unuchek PhD, doctorate [19].

This effect opens up the possibility to polarize a population of specific spin oriented carries with a magnetic field. As well as the possibility to different devices in spintronics such as a spin-polarized laser.

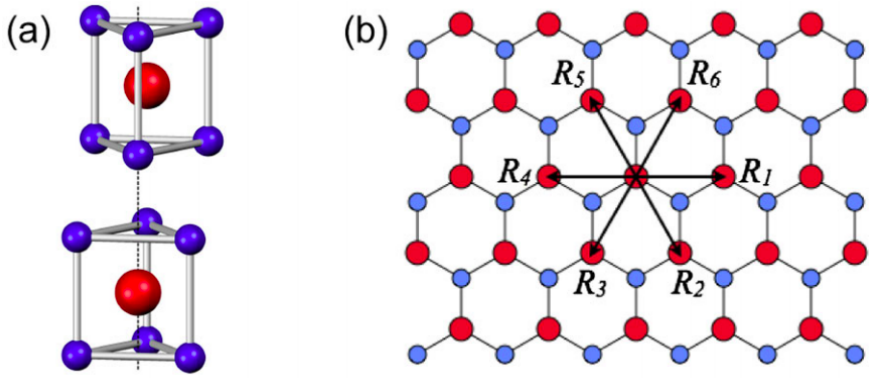

Figure 4: (a) The unit cell of bulk 2H-MoS2. (b) Top view of the MoS2 monolayer. Figures from [4].

2.3 Excitons

Excitons are bound pairs of an electron and a hole. Tipically in semiconductor materials an absorption of a phonon (with higher energy than the band gap) by an electron promotes this electron to the conduction band and creating a hole in the valence band. The two particles, before decaying, can form an excitonic bound state, which has a certain lifetime before decaying [8].

There are many different ways that excitons can exist, Figure 5a summarizes those possible excitons bindings that can exist in nature. Interaction between other excitons, phonons or electrons can induce spin flips and considerable momentum change as a result an exciton may not necessarily be able to recombine radiatively. Such excitons are called "dark exciton". "In general dark excitons are formed whenever the recombination of electron and hole is spin-forbidden or there is a large momentum mismatch" [8]. Other more stable states are also possible, such as inter layer excitons of MoS_2 and WSe_2.

The Coulomb interaction among electrons and holes is strongly screened in bulk crystals, ensuing within the weak binding enery of excitons. In comparison to 3-d-systems, dielectric screening is appreciably reduced in TMDC monolayers, suggesting a sturdy enhancement of the Coulomb interaction. This increases binding energy by several orders of magnitude, separating optical and transport bandgap as proven in Figure 5b [19].

A bound electron-hole pair – is a hydrogen-like quasiparticle and might therefore be excited to distinctive energy levels like Rydberg-like series. This is schematically proven in Figure5c. It is possible to observe that electricity of these excited states strongly deviates from what is predicted for a 2nd-hydrogen atom, specially because of the non-homogeneous dielectric screening within the monolayer limit [19]

Given that excitons are neutral, it is expected that it is not possible to control their flow by applying an electric field. However, excitons have a very well-defined out-of-plane dipole moment which is due to the confinement of different charged carriers. This dipole moment is then sensible to the application of an electric field (perpendicular to the crystal plane) which will shift the exciton energy and thus changing it's diffusion [8].

Figure 6 which comes from Ciarroicchi Phd Thesis [8] schematizes the working mechanism of exciton diffusion modulated by an electrical field, a further more detailed proof of this principle as well the mathematical derivation of exciton diffusion can be found at his thesis.

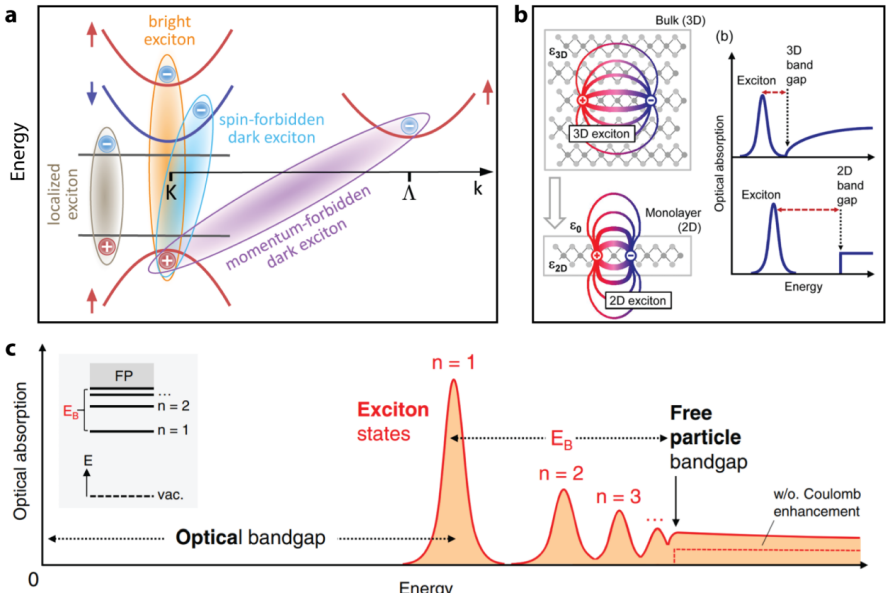

Figure 5: Excitons in single-layers of TMDCs. (a) Different types of excitons and band structure of a tungsten-based TMDC monolayer with spin-forbidden lowest energy transition. (b) Excitons in bulk (top) and monolayer (bottom) have different energy spectra (left) due to the change in the dielectric environment. (c) Typical absorption spectra of a TMDC monolayer revealing exciton ground and excited states. Figures from [5] [6] [7].

At the image there is a main blue center of exciton generations, and it's diffusion across the hetero structure. The presence of a electric field can either block or facilitate the diffusion of those excitons, that "could then be used to realize a switching action for excitons, i.e. an "excitonic transistor", that can stop or allow the flow of an exciton current" [8].

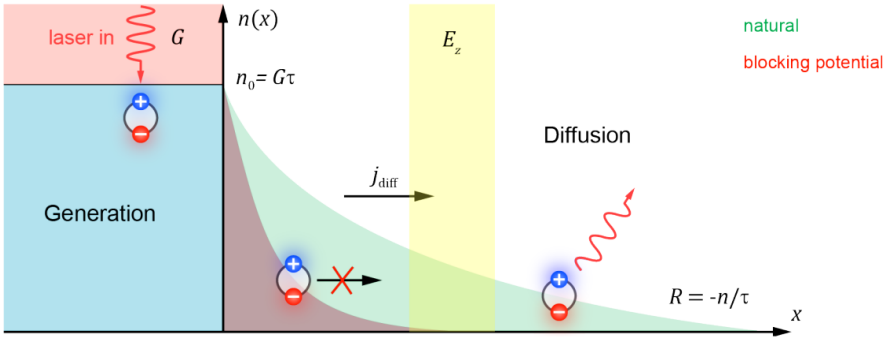

Figure 6: Simulation of exciton diffusion [8].

2.4 Electrical properties

Field effect transistor (FET) is a three-terminal device where the electrical flow between source and drain is tuned and controlled by the gate. As is shown in Figure 7 a), drain and source are separated on two sides of the device while a semiconductor channel is sitting in between. By applying a DC bias on the gate (V_{gs}), Fermi level of the semiconductor is shifted, available carrier density changed, and thus the channel is opened or closed. When additional drain voltage (V_{ds}) is applied, carrier flow inside channel can be modulated by the gate voltage [20], Figure 8 schematises this idea.

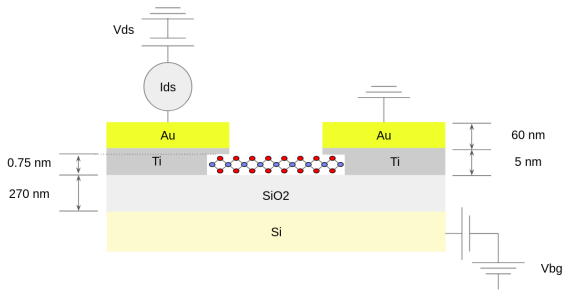

(a) Schematic of a FET device, representative scale

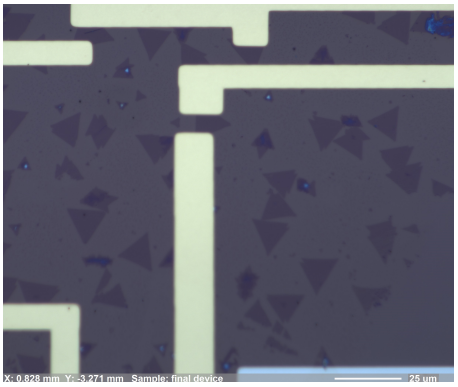

(b) Optical microscope of a fabricated FET device. Metallic contacts are in gold color, MoS_2 channel is the connected triangle, substrate is SiO_2.

Figure 7: Scheme and Optical microscope image of a fabricated FET device.

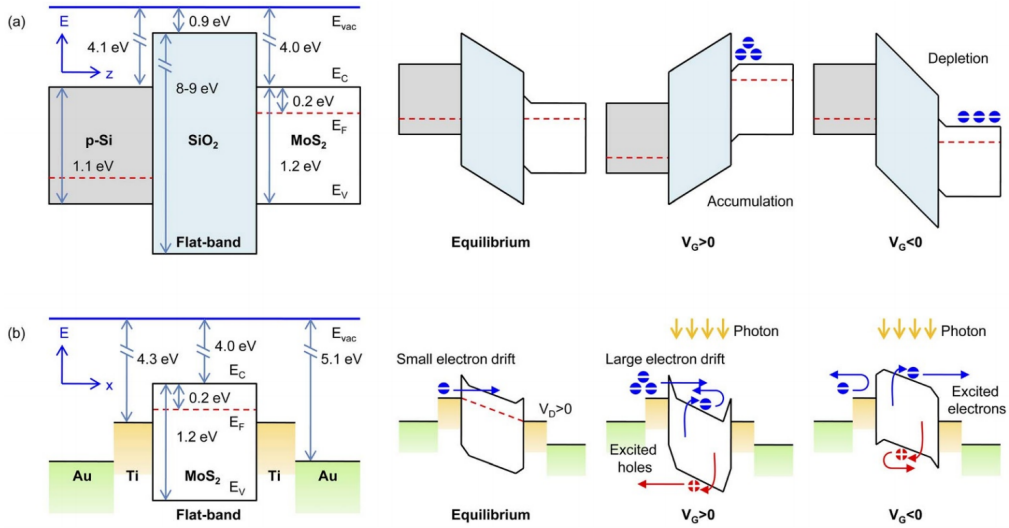

Figure 8: Energy band diagrams of MoS2 FET. [9].

Electrical performance of a FET can be denoted through its transfer characteristics in which the drain-to-source current (I_{ds}) is plotted versus the gate voltage (V_{gs}) or by the output characteristic where the drain-to-source current (I_{ds}) is plotted versus the drain-to-source voltage (V_{ds}). Many important parameters can be calculated from the I_{ds}/V_{gs} curve, including carrier mobility, threshold voltage (V_{th}), and on-off current (I_{on}/I_{off}), while from I_{ds}/V_{ds} curve, the contact resistance and conductance of the devices can be obtained [20].

Carrier mobility can be obtained using the following equation:

$$\mu = \frac{g_m}{C_{OX} V_d} \frac{L}{W} \tag{2}$$

In which g_m is the trasconductance obtained from the slope of transfer curve:

$$g_m = \frac{\delta I_{ds}}{V_{gs}} \tag{3}$$

C_{OX} is the capacitance per unit of area of SiO_2, V_d is the applied drain voltage, L and W represent the effective length and width of the channel. The threshold (V_{th}) voltage can be calculated via the trasconductance curve.

The characterized FET is a degenerately doped Si substrate as a back-gate, and the devices are fabricated on top of the SiO_2 layer covering the wafer. When a voltage difference is applied between the channel material and the back-gate, a charge density n is induced in the semiconductor, according to the relation:

$$ne = C_{BG}(V_{BG} - V_{BG}^0) \tag{4}$$

With V_{BG} is the charge neutrality voltage and C_{BG} is the capacitance between the metal plate of the gate and the channel which is calculated by summing in series the oxide capacitance C_{OX} and quantum capacitance C_Q [8]:

$$\begin{aligned} C_{OX} &= \tfrac{\epsilon_0 \epsilon_{SiO_2}}{d} \\ C_Q &= e^2 Dos(E_F) \end{aligned} \tag{5}$$

In which ϵ is the relative permittivity of the given material, d is the distance, e is electron charge and $Dos(E_F)$ density of states as a function of the Fermi energy E_F. Considering equations 5 into 4 the density and electric displacement field D on the channel are given by [8]:

$$\begin{aligned} ne &= \tfrac{C_Q\ C_{OX}}{C_Q + C_{OX}}(V_{BG} - V_{BG}^0) \\ D &= C_{OX}\tfrac{eV_{BG} - V_{BG}^0}{e} \end{aligned} \tag{6}$$

A MoS_2 FET device also has applications due to short channel effect in transistors, the miniaturization and integration process of microelectronic devices has reached the limit due to the quantum confinement effects when the transistor dimensions approach atomic level. The resulting short channel effect (SCE) can be quantified by the natural length λ:

$$\lambda = \sqrt{\frac{\epsilon_{ch}}{N\epsilon_i} t_{ch} t_i} \tag{7}$$

With ϵ_{ch}, ϵ_i, t_{ch} and t_i are the dielectric constant and thickness of the channel (gate insulator) respectively, and N is the effective gate number of the transistor . λ has to be decreased in order to diminish the short channel effect. An increase in gate number would introduce industrial complexity while reducing the insulator thickness would risk a higher leak current. Therefore, thinning the channel material becomes the only attractive way to minimize the device size without short channel effect. In this regard, two dimensional materials, with nanometer of thickness and micrometer of lateral length as well as good mechanical and electrical properties, have a huge potential for FET applications [20]. Another interesting application for MoS_2 FET devices are monolithic integration on SiO_2 substrate, the idea would be create many step layer of FET devices creating a 3D transistor (whereas in the sillicon counterpart it's limited to the Silicon substrate).

2.5 Chemical Vapor Deposition

Chemical vapor deposition (CVD) is a versatile method suitable for the manufacturing of coatings, thin films, 2D materials, III-V materials, powders, fibers, monolithic components. This generic technique also allows to

deposit most metals onto a substrate and is an essential technique for materials science and semiconductor industry. CVD can be understand as the deposition method where, a precursor is deposited onto a solid heated surface (or substrate) which then reacts with another metallic precursor resulting in an another organic volatile product and metallic product which is deposited onto the substrate, equation 8 summarize this idea [21].

$$(CH_3)_nA + (CH_3)_mB \rightarrow AB + (CH_3)_{m+n} \tag{8}$$

CVD has several advantages which makes it the most preferred process in many cases:

- It is not restricted to line-of-sight deposition.
- The deposition rate is high and thick coatings can be readily obtained.
- CVD equipment do not need ultra high vacuum to work, and generally can be adapted to many process variations

However, the most important drawback is the high temperatures needed in order for the reaction 8 to work and be efficient. Temperatures usually start at high temperatures, and most polymer substrates do not withstand such high temperatures [21].

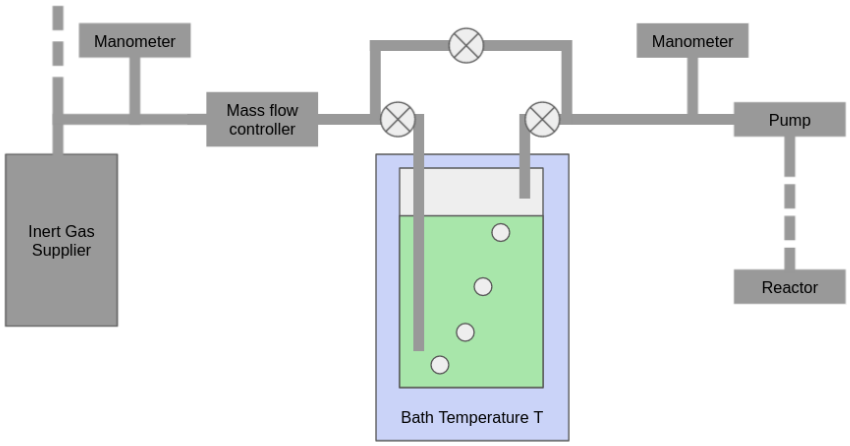

Figure 9: Overview of how a Bubbler works.

Although CVD reactions can be simplified into a vapor-vapor reaction (as noted in equation 8) the reaction mechanisms are way more complex and cannot be well understood without mentioning the transport mechanics that occur. Firstly (refer to Figure 9) the precursors must be flown inside the reaction chamber, in order to do that the bubbler usually receives an injection of a inert gas with a measured pressure and flow rate, this gas creates bubbles in the bubbler (in order to properly dissolve the liquid precursor and maintain an ever state of gas saturation), which is then flown to the reactor a mixture of inert carrier gas and the saturated vapor pressure of the precursor.

To precisely determine the amount of flown precursor in the reactor, it is necessary to very well define: the temperature of the bubbler (Refer to image 9) which gives the saturated vapor pressure, the height of the tube going inside the precursor - which is assumed to be sufficiently large in order to maintain a saturation state ;

and the pressure of system (P_0) in relation to the vapor pressure of the precursor (P_R), if it is $P_0 > 3P_R$ then the flow or reagent is given by [22]:

$$F_R = F_C \frac{P_R}{P_I} \tag{9}$$

Where F_R is the flow of the reagent (or precursor) and P_I is input pressure of the carrier.

Before entering the reactor the other gases mix in the gas lines arriving (as one hypothetically homogeneous gas) at the gas inlet. From now on, the type of the reactor greatly influences the flow of precursors and therefore the kinetics/thermodynamics of the reactions. The first large-area epitaxial monolayer [11] of MoS_2 that has been published has been done in Lanes group using a lab made horizontal reactor (refer to Figure 10). The gas arrives from the gas inlet into the reactor, which is then flown towards the center of the reactor where it is heated with hot walls (temperature varying from room temperature to 1100 degrees Celsius), reacts with the substrate deposing the desired material, the rest products are then pumped out of system via the gas outlet.

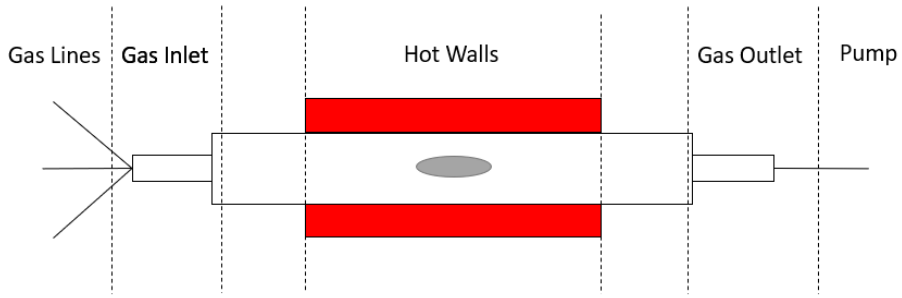

Figure 10: Overview of a horizontal reactor

This system works fair well and give good results for academic purposes, the gas mix well before entering the system and, it is properly heated before the reaction occurs. The substrate position can vary according to the growth purpose (may stand up, or be lightly tilted). But for industrial purposes, this system isn't ideal because of the difficulty for large scale growth, increasing the number of wafers inside the reactor potentially decreases the material deposited on the wafers with less precursor supply. This system usually follows a homemade software, is necessary a lot of manual intervention - which is mostly undesired in an industrial environment.

Figure 11 represents an Aixtron reactor, which can be more suitable for industrial applications. Aixtron is a company which develops different types of CVD reactors, their main niche is for III-V material growth, in 2017 Lanes laboratory ordered an Aixtron machine destined to synthesize 2D Materials which use very similar principles as the ones used in III-V synthesis. As mentioned in the vertical reactor, the gases mix at the gas inlet (which can be shaped with different type of and size of holes for better flow of material), usually the gas inlet is equipped with a heater which grants a desired temperature of the precursors even before getting into the reactor, the gas is then flown towards the suscpetor which holds the Wafer (as noted from the image on the left, the suscpetor can have different type of holders, capable of holding one 4-inch wafer, or three 3-inch wafer or six 2-inch wafer), the susceptor is also equipped with a heater granting a proper substrate heating. The residual products are then flown towards the gas outlet via some small concentric holes. Some of those industrial machines are equipped with different types of tools, for instance, the susceptor may be equipped with an Argus tool which permits to draw the temperature profile across the wafer in-situ, or even an Laytech Epicurve which gives in-situ curvature of the wafer. For even greater cleanness of the material deposited the

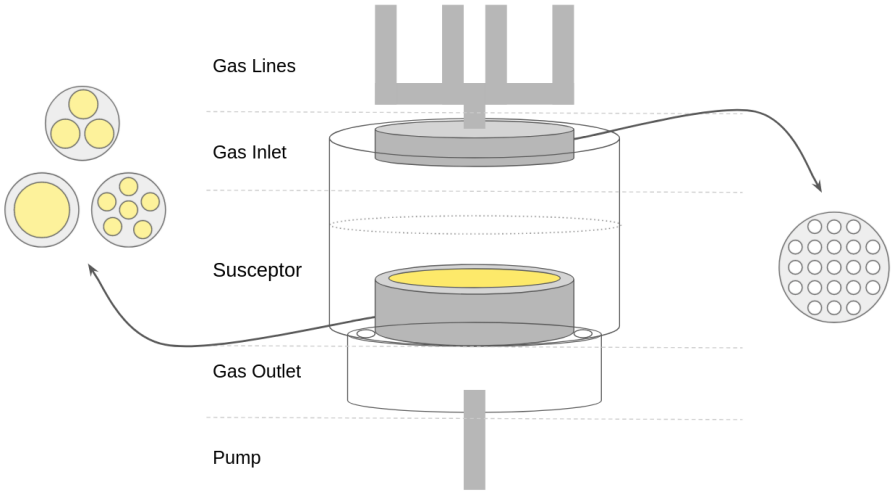

Figure 11: Overview of an Aixtron reactor

reactor is inside a glove box (which is am ambient with very low concentration of oxygen and high concentration of inert non toxic gases). Lastly this comes with a software which permits to do multi step growth, trace the variation of different parameter and even set multi step cleaning process of the reactor (with possibility to use plasma). For this given reasons, usually aixtron machine is preferred to for industrial scale growth.

The main drawback of using an industrial machine like this are that those machines are usually not designed for the nuances of 2D Material Growth, for instance, the usage of S precursor may etch a metallic surface and contaminate the deposition. Sometimes is also interesting to flow H_2O or O_2 along with the precursors[23], but this may oxidize the metallic parts of the reactor.

The thermodynamics in Chemical Vapor Deposition are defined by Gibbs Free Energy (G):

$$\Delta G = \Delta H - T\Delta S \tag{10}$$

Where H is enthalpy, T the temperature and S the entropy. In order for a reaction to occur ΔG must be lesser than 0 [24]. Considering the equation 8 we can define the kinetics of the reaction as:

$$K = \frac{P_{(CH_3)_{n+m}}\ a_{AB}}{P_{(CH_3)_nA}\ P_{(CH_3)_mB}} \tag{11}$$

Where P_i is the partial pressure of gas i and a_j is the activity of solid j. Permitting to write the equation 10 as:

$$\Delta G = \Delta G^0 + RT \ln K \tag{12}$$

Where R is the gas constant, and ΔG^0 is reference thermodynamic point (300K and 1atm). As mentioned before, generally the deposition of a metal is not done by one single reaction, usually there are various intermediate steps with numerous types of reactions, and since there is a lack of understanding on CVD thermodynamics on TMDC, to elucidate this lets consider the CVD of GaN, according to [25] there are 18 gas phase possible reactions of GaN, not only that, but the surface also is prone to nucleation and catalysis of different depositions with up to 52 surface reactions. Also, equation 11 doesn't consider the influence of flow rate of the gas precursors.

It's possible to rewrite equation 11 as a function of the flow rates, considering Dalton's law:

$$K = \ln \frac{\eta_{(CH_3)_{n+m}} \ a_{AB}}{\eta_{(CH_3)_n A} \ \eta_{(CH_3)_m B}} \tag{13}$$

With η_i as the flow rate of material.

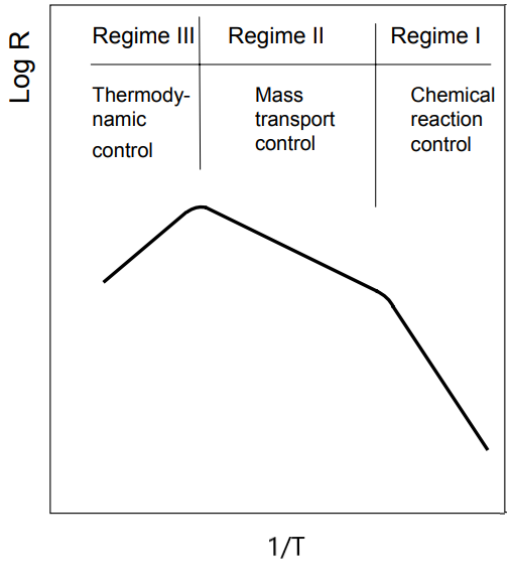

Figure 12: Temperature dependence of deposition rate on a globally exothermic CVD reaction. Figure modified from [10]

Deposition rate with respect to temperature represented in figure 12. Although it's desired that deposition rate of 2 materials to be very low in order to deposit only mono layers, this figure elucidates the different regimes that control the kinetics of this process with respect to temperature. To explain the different regimes consider Figure 13 :

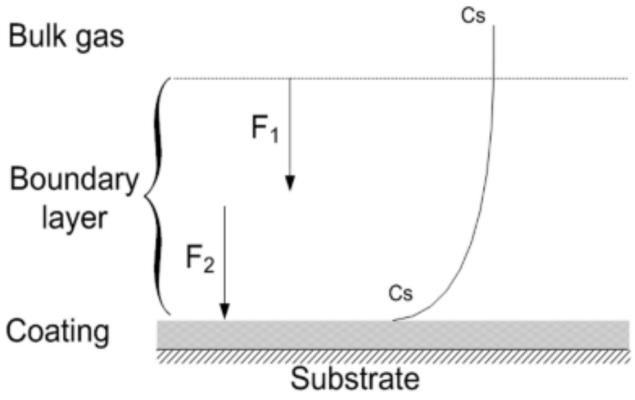

Figure 13: Schematic of growth process model [10].

According to Thermodynamics and Kinetics of Chemical VapourDeposition [10] it's possible to model the flux (F_1) of mass transport from the gas phase to the substrate surface, whereas C_G and is the concentration of

reactant gaseous species in the bulk gas phase and C_S is the concentration at the surface of the substrate can be is written as [10]:

$$F_1 = h_G(C_G - C_S) \tag{14}$$

h_G is defined as the mass transfer rate constant and can be determined by the boundary layer equations:

$$h_G = \frac{D}{\delta} \tag{15}$$

Where D is the diffusion coefficient for the reactant gaseous species and δ is the thickness of the concentration boundary layer. The flux (F_2) of the reactant gaseous species consumed on the substrate surface, with k_S as the heterogeneous reaction rate constant, can be equation-ed as [10]:

$$F_2 = k_S C_S \tag{16}$$

Under steady conditions ($F_1 = F_2$), the relationship of C_S and C_G is obtained [10]:

$$C_S = \frac{C_G}{1 + k_S/h_G} \tag{17}$$

3 Methods

This master thesis is based on 4 main pillars: material synthesis, material characterization, device fabrication and device characterization. The following section will describe and review some general aspects of the employed experimental techniques.

3.1 Synthesis

The following sub-section will detail the experimental procedure that has been taken to growth MoS_2, every step will also be further detailed and justified according to theory and or recent papers on the given subject.

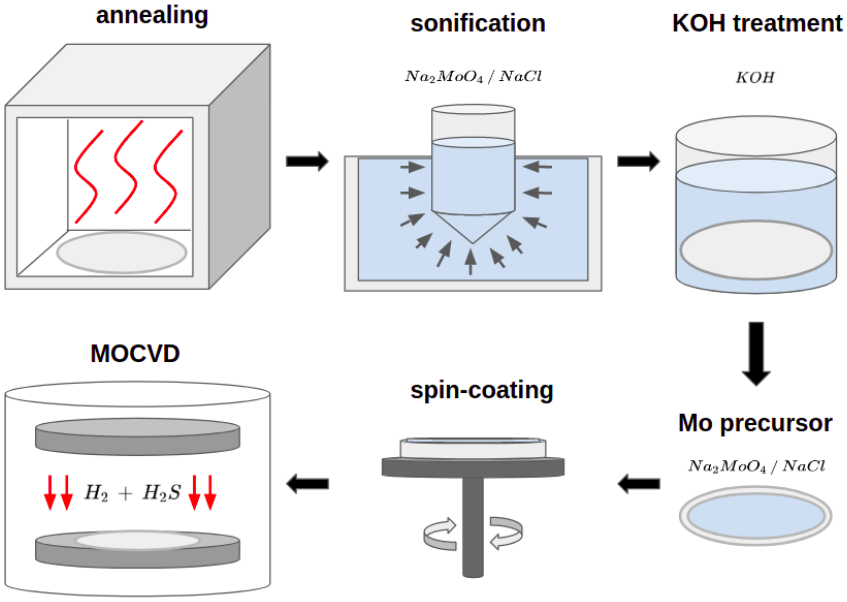

Figure 14: Overview of the experimental procedure.

Figure 14 schematics the experimental procedure taken place to grow the MoS_2 2D material. The first step is to clean the sapphire substrate with acetone/isopropanol/DI-water, followed by **annealing** the sapphire substrate in high temperatures (1000°C) in air for 1 hour. After annealing, a solution of $Na_2MoO_4/NaCl$ goes into **sonification** for a couple of minutes. The substrate is then put in **KOH treatment**, for a few minutes. Which is then homogeneously added the **Mo precursor** with the aqueous solution of Na_2MoO_4. To after it will be **spin-coated** along the sapphire wafer. And the last step is deposition of H_2S precursor inside the **MOCVD** chamber for one hour at 900°C.

3.1.1 Pre-treatment of sapphire substrate

Annealing Annealing the sapphire substrate for MoS_2 growth has been reported in numerous publications [11][26][27][28], the temperature suggested ranges from 1000 °C to 1100 °C, but the time is always reported for one hour. The main purpose of this process is, as suggested, to achieve a clean, atomically flat surfaces [26] [11].

As Dumceno et al shows in Figure 15 annealing has a great importance in well orienting the surface and removing extra planes that might inhibit the MoS_2 growth [29] [11]. Furthermore, the more time or higher the

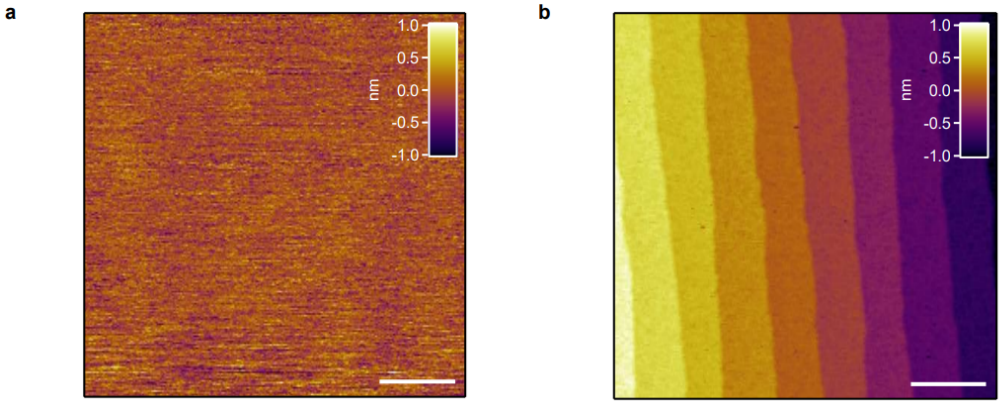

Figure 15: Effect of annealing in air on the morphology of c-plane sapphire. a, AFM image of the as received sapphire surface. b, AFM image of annealed sapphire used here as the growth substrate. After annealing in air, the surface shows atomically smooth terraces [11].

temperature, the better quality will be the sapphire substrate [11].

C-plane sapphire (with hexagonal lattice structure) isn't the only substrate used for MoS_2 growth, there have been reports to also use substrates like: Si, quartz, mica, Au, h-BN and Graphene [30] [31] [32] [33]. Although c-plane sapphire (with lattice constant $a = 4.814$Å) has a relatively high lattice mismatch with MoS_2 ($a = 3.212$Å) it is the preferred because the atomic orientation of c-plane sapphire is very similar to MoS_2 (since they are both hexagonal)[11].

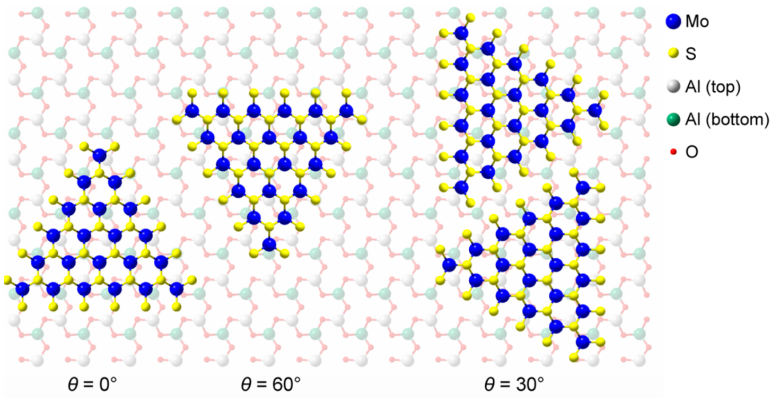

Figure 16: Schematic drawing showing the top view of relative lattice orientations between monolayer MoS_2 and c-plane sapphire. Modified from [11].

Figure 16 schematizes the lattice orientation between MoS_2 and c-plane sapphire, the stacking orientation of $\theta = 0°$ and $\theta = 60°$ are the preferred growth orientation of the crystals, the orientation of $\theta = 30°$ and it's respective of $\theta = 90°$ are the second most thermodynamically stable orientation. Those results have not only been experimented observed by Dumceno et al, but also DFT simulations have been done to show that the nature of those interactions are in fact vdW [11].

Sonication Although sonication isn't mentioned as much as annealing, in Cun [26] has been mentioned as a step to clean the sapphire wafer which is based on cavitation which removes surface contamination. In general, sonication is used in nanotechnology for evenly dispersing nanoparticles in liquids. And it is also used, as it

has been shown in [34] to reduce nanoparticles size in aqueous solutions. The intention here is by giving high energy waves the solution will be cleaner and will have reduced nanoparticles size.

KOH treatment KOH or $NaOH$ pre treatment has been mentioned by few authors [26][13][12] as an important step towards a homogeneous deposition of precursor. Figure 17 shows the effect of prolonged contact of Si wafer with a solution of $NaOH$.

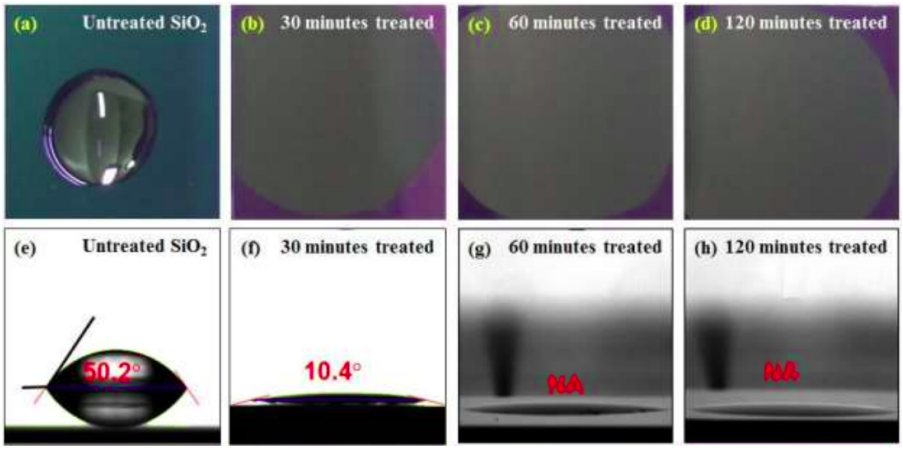

Figure 17: Contact angles and uniformity of MoS2 before and after NaOH treatment. (a) Photograph of SiO2 before and (b-d) after NaOH treatment. (e) Contact angle for untreated SiO2. (f-h) Contact angles of treated SiO2 for 30, 60 and 120 minutes respectively. Modified from [12].

Since the molybdenum precursor is liquid, a strongly hydrophilic surface is necessary for a good spin coating. Therefore, prior to spin coating, the Sapphire substrate is treated with as solution of KOH (3% in weight) to increase its hydrophilicity (therefore decreasing the contact angle - as suggested in Figure 17).

3.1.2 Precursors

Mo Precursor The choice of precursor is quite different among different works, some chose to work with MoO_3 precursor [28][31][35][36][15] others tend to use $Mo(CO)_6$ [11][30][32][13][37], this work has followed the same of route of Cun [26] and Boandoh [12], therefore $Na_2MoO_4/NaCl$ is the chosen precursor. The reason behind that is because, since the growth is done in a Aixtron machine, MoO_3 is opted out because the machine doesn't have this precursor installed. $Mo(CO)_6$ is opted out because of the possibility of carbon contamination which greatly reduces the growth of the material and also has the possibility to render the electrical component useless.

NaCl is used to increase lateral growth of the MoS_2 crystals. Kim [13] has made a study in the implications of alkali metal halides towards suppressing nucleation of MoS_2, resulting in the increase of lateral dimensions of single crystalline domains by more than 2 orders of magnitude.

Although suppressing the nucleation of the crystal might suggest that it reduces the growth of MoS_2 material - it does, in fact, greatly reduce the number of crystals in the material but it also greatly increases the lateral dimension of those crystals. As it is suggested in the results shown in Figure 18

As stated in Kim et al work [13], it is not very well known the underlying mechanism of the usage of alkali metals in MoS_2 growth, it has suggested that, those metals instead of acting as desiccants suppressing

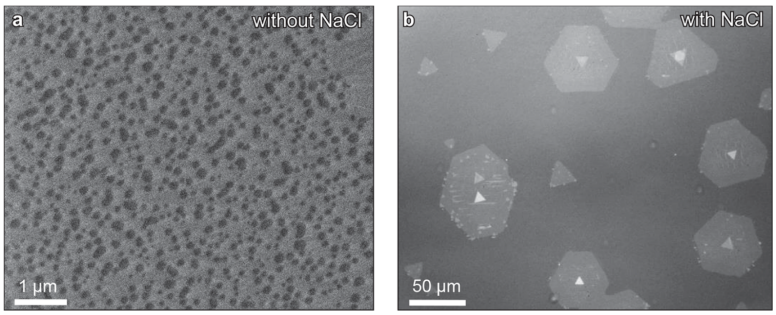

Figure 18: (a) SEM image of MoS_2 (b) Optical microscope image of MoS_2 grown on sapphire during $NaCl$-assisted growth. Figure from [13]

nucleation and enhance two-dimensional growth in the conventional chemical vapor deposition of TMDCs. One other possible explanation is that a planar molecule can act as a seeding promoter because it can stabilize the two-dimensional nuclei due to its geometry [13].

Spin coating A uniform layer of molybdenum precursor is done with, which is fundamental for a homogeneous MoS_2 film. This procedure has been done by Cun [26] and Boandoh [12].

The speed and time greatly influences on the homogeneity of solution in the wafer, as well as the thickness of the precursor.

S Precursor The reaction conditions in Aixtron system is different from what is observed in the literature, Mo precursor is solid phase, S precursor is in gaseous state and fluid dynamics of this shower head MOCVD greatly influences the reaction inside the reactor.

Since there are few reports of growth with this machine, the S precursor choice, the usage of H_2 and the time of reaction has been heavily influenced from other reports of CVD/MOCVD growth of MoS_2 thin films [26][12]. The H_2S is one of the most used precursor for CVD and MOCVD growth and its interaction with H_2 has been studied in previous works [11]. H_2 is an important gas in the reaction as it was studied by Li work et al [38] and stated in previous work by Boandoh el al [12], hydrogen is a reduction agent for molybdenum oxide described by Equation 18:

$$MoO_4 + 2H_2 + 2H_2S \rightarrow MoS_2 + 4H_2O \tag{18}$$

Hydrogen also is as a chemical etchant, according to previous Li [38] report, excess H_2 may promote desulfurization, as suggested by the Equation 19:

$$n(MoS_2) + \frac{(2-x)y}{2}H_2 \rightarrow n(MoS_x) + (2-x)H_yS \tag{19}$$

Therefore an adequate flow of Hydrogen is important to promote either a good growth and reduce defect apparition in the material. Time is also a relevant factor and it has been studied by Lanes laboratory, the greater the time does not necessarily lead to bigger grains.

Temperature is also a relevant factor, precedent reports [26][12][11] suggest reaction temperature at around $900°C$. Although pressure is an important thermodynamic variable, it is rarely a cited factor.

.

3.2 Material Characterization

In this section the techniques used to characterize the materials grown will be described. The main focus will be on how those techniques can give crucial information about MoS_2 crystal growth.

3.2.1 Optical micrography

Optical Microscope is one of the main source of information on MoS_2 monolayer growth, with it, it's possible to infer if there has been any contamination on the sample or if the deposition is homogeneous. It's also possible to quantify information on crystal grown itself, like nucleation density, crystal size, crystal orientation, if there has no growth or mono layer growth and growth area on the sample.

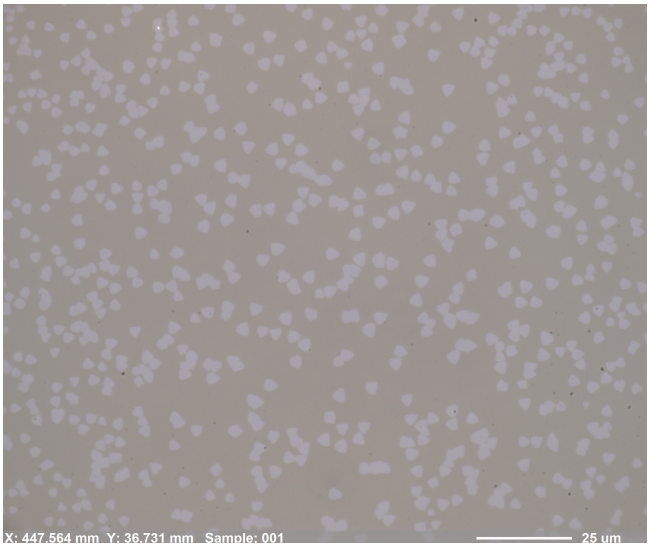

Figure 19: Optical Microscope ($x100$) of MoS_2 growth on c-plane Sapphire.

Figure 19 shows an optical micrograph of one of the growths made during this master thesis. Using software such as ImageJ/Fiji (version 1.53c) it's possible to quantify the crystal growths of this sample. Figure 20 represents a few of data treatment and data analysis of the given sample. This process is crucial in order to precisely quantify the impact of modifying the thermodynamic variable in growth.

It's also important to notice that this technique is not always precise, as seen in figure 20c the software couldn't separate the merged flakes together therefore giving a bigger surface area to a conglomerate of particles. Or in the Figure 20d some crystals shows different orientations but the software may count the same angle for them. Also in-homogeneous light across the sample, may also heavily influence the reliability of the software, but this can be solved if there is a subtraction from the raw data of a background image obtained without laser illumination, to account for ambient light noise improves the results. In general, this type of software can be very useful for data treatment but must be used with caution.

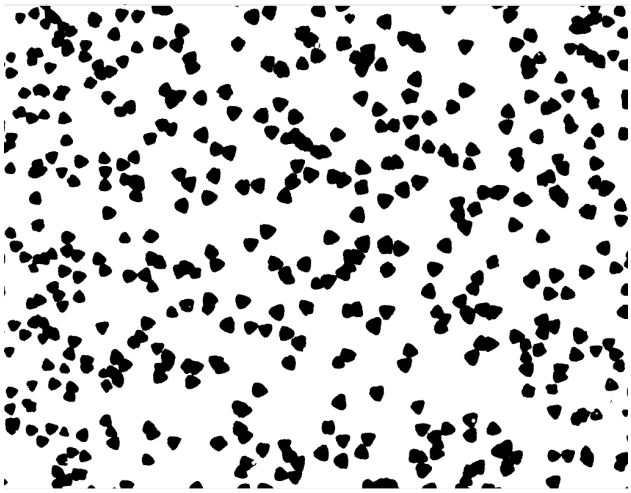

(a) Figure after Threshold filter.

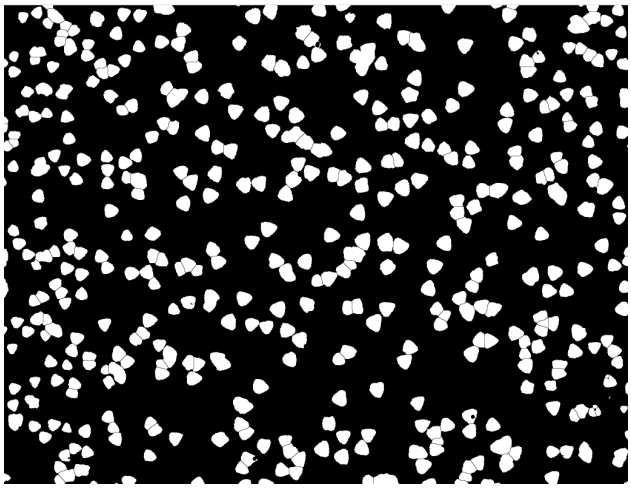

(b) Figure after water-shed in order to be differentiate particles

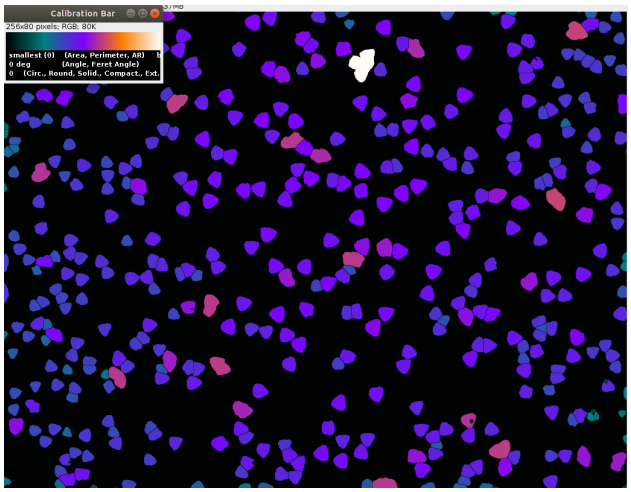

(c) Quantification of triangles by area.

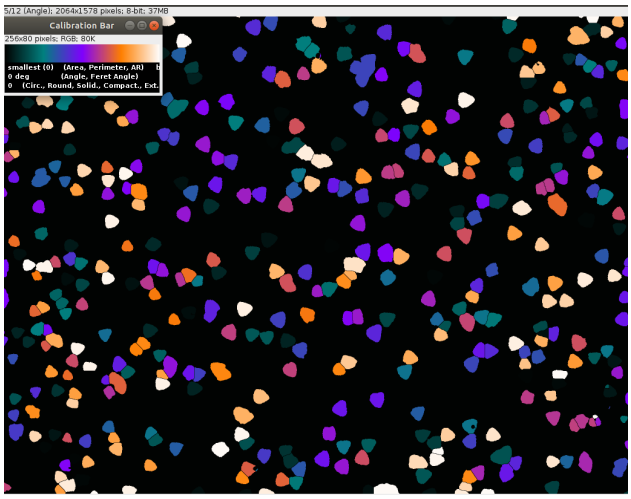

(d) Quantification of triangles by orientation.

Figure 20: Different analysis and data representation of a given sample.

3.2.2 Scanning Electron Microscopy

Scanning electron microscopy (SEM) is a important tool because it allows to have resolution all the way to nanometer scale and due to the way the technique works, it is also possible to visually differentiate components in a given sample according to their weight mass (the higher the weight mass, the more light it emits back, therefore they have a higher contrast compared to other elements).

Although MoS_2 is a conductive material the growth occurs on sapphire (insulating substrate), due to this

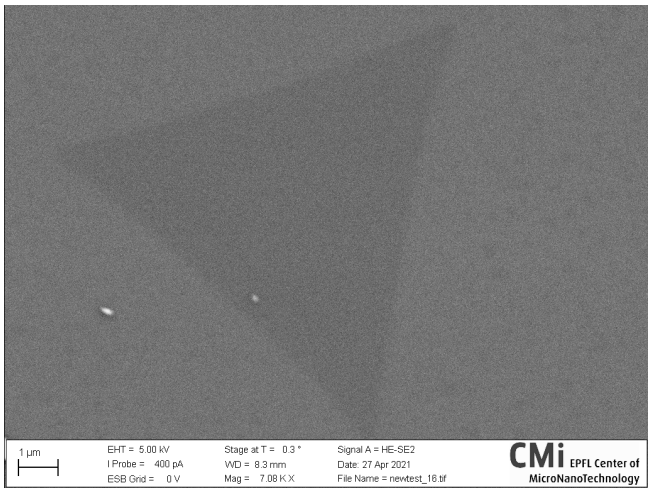

Figure 21: Scanning Electron Microscope image of Sample, resolution can go closer to 1nm, the higher the mass the darker the figure is.

SEM is hard to use and needs extra care compared to the silicon counterpart (due to low signal to noise ratio).

3.2.3 Energy Dispersive X-ray Spectroscopy

EDX is an important tool because when combined with SEM it is used for the elemental analysis or chemical characterization of a sample giving accurate results to the atomic percentage of elements.

Since Sapphire is not a conductive substrate and the deposition of MoS_2 is usually only one layer, EDX also needs extra care, and has been used just to better understand possible contamination and patterns that occurs in the material growth.

In order to better increase the visualization of the sample a conductive tape has been put into contact with the sample in order to make it more conductive, the voltage was usually $1keV$ and current at around $100pA$ - other techniques has also been used in order to reduce substrate charging (event in which the isolant substrate starts accumulating charges and works as an mirror for the incoming electrons), like continuous averaging, focusing on very small sample areas and longer accumulation time with weaker laser.

3.2.4 Atomic Force Microscope

Atomic Force Microscope is a type of scanning probe microscopy which uses a very sharp tip in order to probe a sample, by scanning the surface while monitoring the deflection this tool allows to give relevant height information up to sub-nanometer precision [8] [39].

AFM was used to measure the height of individual flakes of 2D crystals to determine the number of atomic layers, also it was used to assess their cleanness and to check for microscopic cracks and defects that would be impossible to observe by optical microscopy [8].

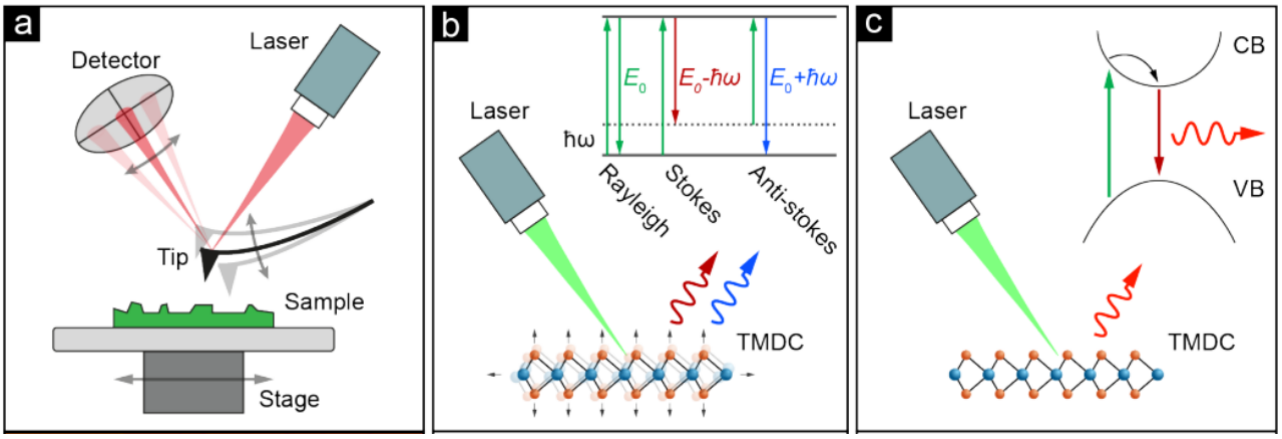

Figure 22: Material characterization techniques: (a) AFM scanning: principle of operation. (b) Raman spectroscopy: schematic depiction of Raman scattering. (c) PL spectroscopy: general principle of PL emission. Figure modified from [8].

3.2.5 Photoluminescence Spectroscopy

Photoluminescence (PL) is a technique that analyzes the light emitted from a semiconductor structure. Carriers are photoexcited and move from one energy level to another. The energy of a particular luminescence transition depends on the relative spacing of the initial and final energy states. These states can be impurities or localized defect exciton states [40].

The advantages of PL are to give a lot of information very quickly and easily, it has the ability to measure non-radioactive recombinations, to measure the band gap energy, to determine the crystal quality and is a specially used technique because it is non-destructive [40].

For the purpose of understanding a 2D Material Growth Photoluminescence can be used to analyze parameters such as strain, doping, disorder, in MoS_2 the PL spectrum is dominated by excitonic species, mainly the neutral and charged excitons. By looking at their relative intensity and emission energy for example, information on the doping of the crystal can be obtained [8]. Figure 23 represents the optical band gap of the material MoS_2, the electronic band gap (Eg) represents the energy necessary to form a electron-hole pair, the exciton biding energy forms this electron hole in a more stable quasi particle, A exciton is the exciton with lowest energy that appears in material and B exciton is the second lowest energy (due to spin orbit coupling, refer to section 2.2).

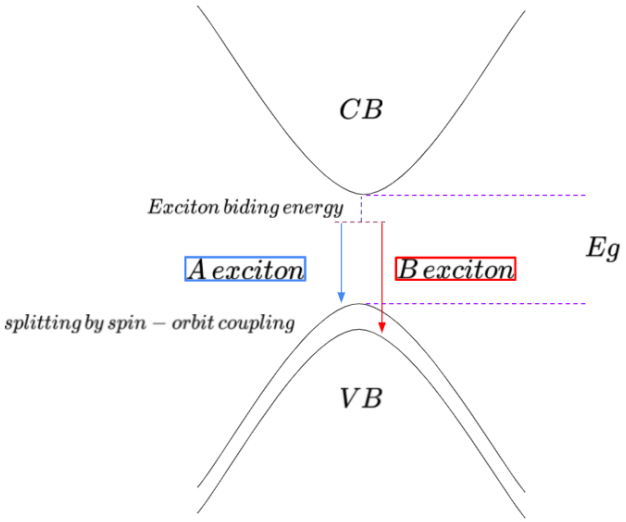

Figure 23: Energy schematic of optical and electronic band gap. CB stands for conduction band and VB to valence band.

3.2.6 Raman Spectroscopy

Raman spectroscopy is a non destructive technique that permits to characterize a materials phonons mode. It's working mechanics is based on the analysis of the spectrum of light scattered from the sample upon optical excitation [8].

Upon exciting a sample with a laser beam the energy of the photons are absorbed by the electrons of the material, this energy then is used to excite the electron to an excited state which is "later decayed to lower energy one by emitting scattered light. If the process is elastic (Rayleigh scattering), the emission frequency is the same as the excitation, producing a bright spectral line at the same energy of the laser"[8]. But it is also possible that this process is inelastic which leads to creation of phonons and thus generating additional Raman peaks[8].

For 2D Materials Raman spectroscopy can give information used to evaluate the number of layers in the crystal, due to the coupling between electronic transitions and phonons [8]. It can also be used to asses the crystalline order of the sample, such as the presence of defects or different crystal phases, which would alter the normal vibrational modes of the crystal.

Specially in the case of MoS_2 the observed excitation modes are A_{1g} (out of plane vibration mode) , E^1_{2g} (in plane vibration mode) and $2LA$ (second order longitudinal acoustic phonon). Where as the latter is defined by coherent oscillations of atoms of the lattice out of their equilibrium positions, and the first two are out-of-phase movements of the atoms in the lattice [41]. Figure 24a) schematizes this modes of vibration and figure b) represents the phonon band structure of MoS_2, the main observed frequencies are at point M, with LA, E' and A'_1 band lines [14].

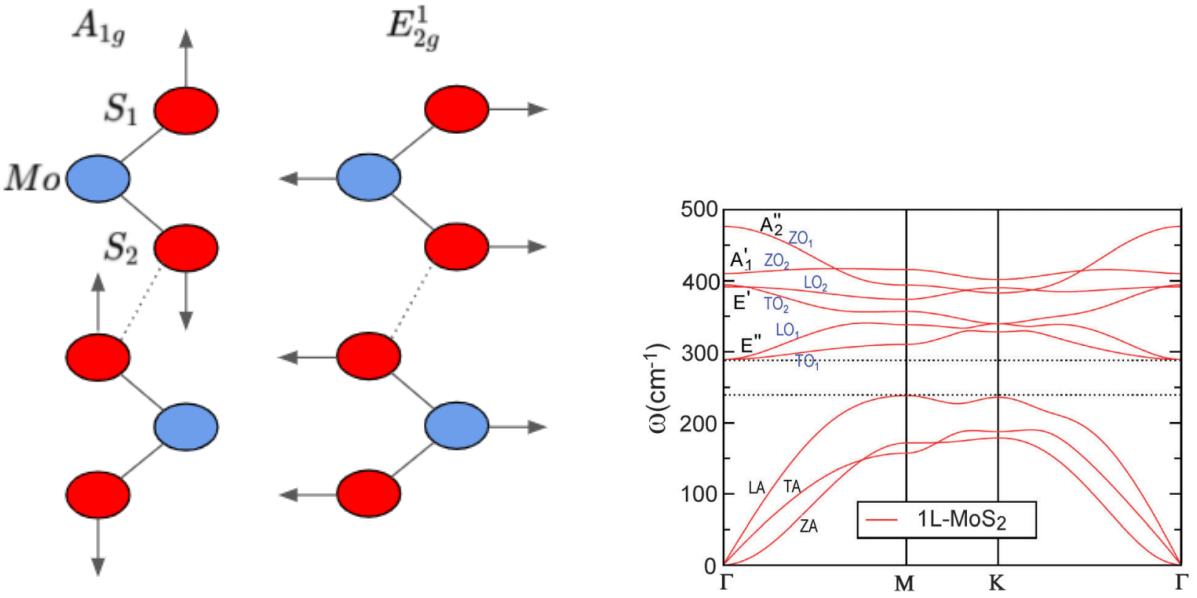

(a) Representation of main phonon vibration modes in MoS_2.

(b) MoS_2 phonon band structure.

Figure 24: Main phonon vibration modes and phonon band structure of MoS_2 [14].

3.3 Fabrication of MoS_2 Field effect transistor

The following sub-section will detail the experimental procedure that has been taken to fabricate the MoS_2 device, every step will also be further detailed according to theory and or recent papers on the given subject.

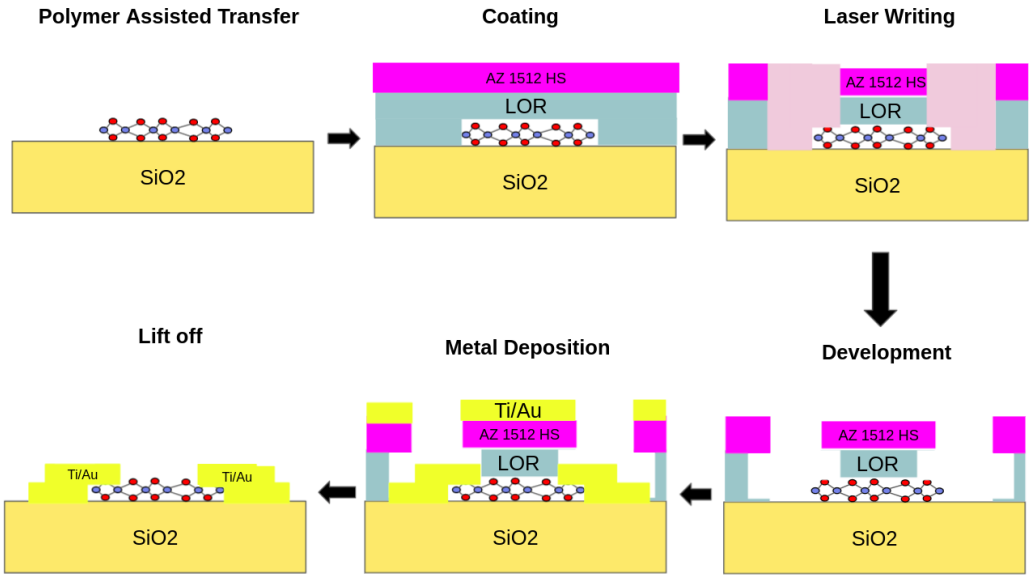

Figure 25: Schematics of Fabrication Process.

Figure 25 schematics the fabrication procedure taken place to create MoS_2 device. The first step is growth of MoS_2 as described in section 3.1, after the crystals are **Transferred** onto a SiO_2 substrate using the **polymer assisted transfer** technique. After that Lift off Resist (LOR - thickness of 400 nm) is spin-coated, and a

Positive Thin Resists for Wet Etching (AZ 1512 Hs - thickness of 1100 nm) is also spin coated. **Laser Writing** is used to exposed the desired pattern, fragilizing LOR and AZ. In the **Development** the sample in exposed to a developer (AZ LOR) which removes the exposed polymers as well as isotropically etches the LOR creating the "undercut". In **Metal Deposition** 5 nm of Ti is deposited and then 80 nm of Au is deposited. In the **Lift-off** process, the sample stays in a polymeric solution for 1-4 days in order the remove the AZ and LOR photo resists of the sample leaving only the desired metallic contacts.

3.3.1 Transfer of MoS_2

The first step towards fabricating a MoS_2 device is to transfer the 2D Material into a proper substrate for electronic applications (Si). There have been numerous reports of different techniques such as: Viscoelastic stamp transfer, Polymer double layer transfer, Pick-up transfer, Wet transfer, PDMS transfer and Double-layer transfer [8][19]. The technique employed here is known as polymer assisted transfer and is schematized in Figure 26. Firstly PMMA A2 in spin coated MoS2/Sapphire at 1500rpm/60s, followed by baking at 180'C for 5 minutes,

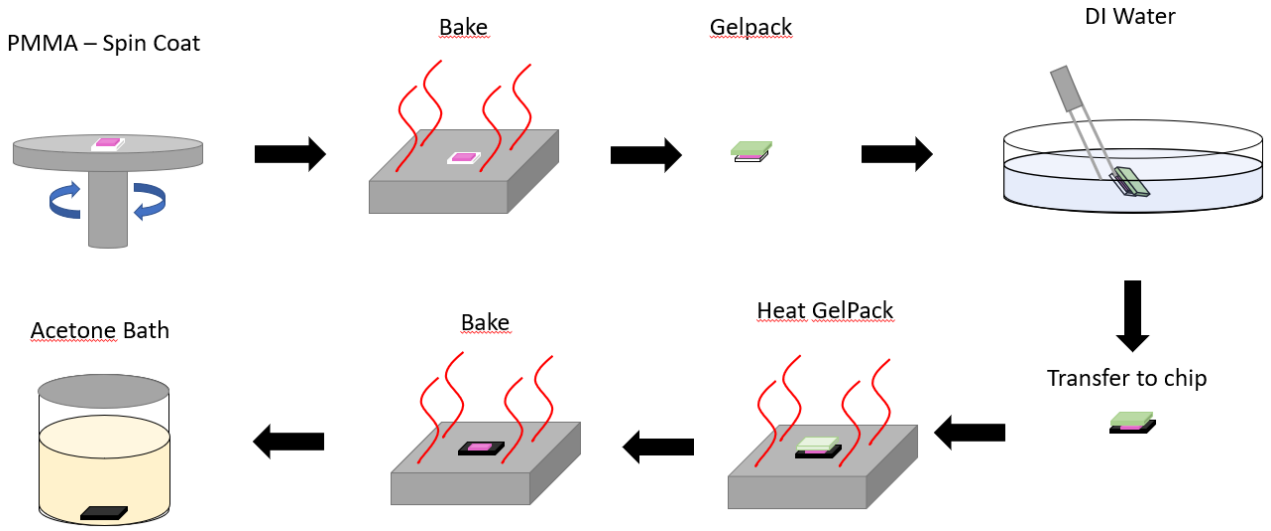

Figure 26: Transfer Overview

then the corners of the sample are scratched so water can penetrate more easily, which after it is cleaned with IPA. A gelpack which is slightly bigger than the sample is cut and place in the PMMA/MoS2/Sapphire (it's recommended in this step to gently press with a tweezer to remove bubbles inside the gelpack). This stack is put under a DI water beaker and using a sharp tweezer the gelpack is pocked on the sides in order to water to penetrate the sample. Remove the gelpack by the corners, dry gently with thin paper, transfer to SiO_2 substrate (remove air bubbles), bake at $55°C$ for 60 min, after which the sample is rinsed a couple of times with acetone and lift off the gelpack in acetone for a few days (2-3).

3.3.2 Laser Writer

Due to irregular flakes produced by MOCVD and the small size of the devices, laser writer become employed as the principle patterning method. Via coating the chip with an electron sensitive polymer (AZ 1512), it's then possible to draw designs on the chip with a laser beam. This beam changes the solubility of the resist, permitting to selectively remove the exposed or un-exposed areas of the resist by immersing it in a solvent. This produces a "mask", exposing the substrate in a few regions, while leaving it untouched in others [8].

The very first stage for any process whether it is metal deposition or etching, is the preparation of CAD file aligned with desired device. Once the desired pattern is designed in PC (Klayout) and exported into appropriate gds format [19].

After coating with resist, the samples are exposed with a 405nm laser and with 70[mJ/cm^2] dose. High quality imaging was also used giving a precision close to $1\mu m$.

3.3.3 Metal Deposition and Lift-off

In order to do an electrical characterization of a desired metal it is necessary to create a metallic contact with the 2D Material and the measurement tool. Au is known to provide a good injection of carries into the MoS_2 flake, but usually it has a bad adhesion, so in order to grant a better contact a tiny layer of Ti is deposited before hand [19]. The machine used is Vistec EPBG500ES and once the deposition is done, the sample is put in acetone to remove the resist, leaving the metal only in the patterned areas [8].

Lift-off is the final step to complete contacts deposition. The following procedure was taken place:

- Rinse the chip a couple of times with acetone to remove AZ photo resist.
- Place in a closed container with polymeric solution and leave from 1-4 days to dissolve LOR and lift off the rest of the material
- Rinse with fresh acetone, isopropanol and dry with nitrogen gun.

3.3.4 Etching

If necessary, the device can be patterned in a particular shape for specific measurements, especially to prevent shortcuts [8] [19].

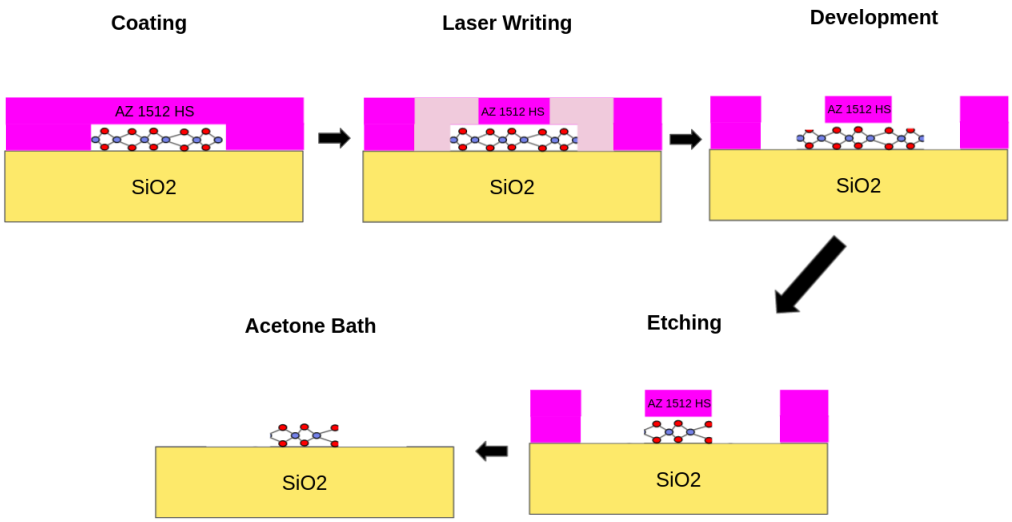

Figure 27: Schematics of etch process

3.4 Electrical Characterization

Before measuring the device it's necessary to connect it to a probe station before, Figure 28 schematizes this process. Firstly the chip must be ready with all it's proper metallic contacts inside it, then it's attached into a 24 gold pin package using silver glue, then using very precise tools the metallic contacts of the chip are connected to the metallic contacts of the package via wire bonding and on the last step the package is connected to a probe station where each leg of the package is associated with a specific number, and thus can be applied a specific voltage.

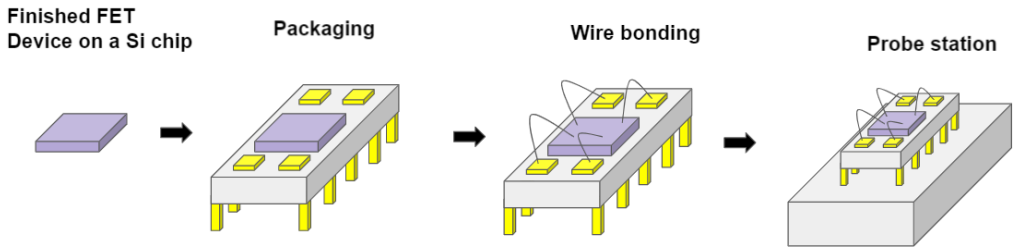

Figure 28: Measurement schematics

The results are then recorded via a labview program that was made in the lab, registering the output variables in order to plot the Transfer and Output curves. It's also possible to do this measurement in a cryogenic environment, thus properly controlling the temperature and registering the different behaviors according to temperature shift.

4 Results and Discussion

In this section the results of MoS_2 thin film growth and device fabrication have been presented. Different morphology of the material, as well as different properties has been presented and discussed accordingly.

4.1 Metalorganic Chemical Vapor Deposition growth

In total, during this work, there has been done eleven CVD growths, ten in aixtron machine and one in a tube furnace. The first few results (1-7) from Aixtron were trial runs in order to understand and learn how to use the machine, as well as how to better clean the furnace for better growth.

4.1.1 Optical Image

MoS_2 present various different morphologies according to growth conditions and sample position, close to the border for example, there is almost no growth due to contamination which inhibits crystal growth. Closer to the center of the sample there is almost no growth as well due to possible inhomogeneity of precursor flow in the center. Figure 29 schematises the main areas of MoS_2 morphology.

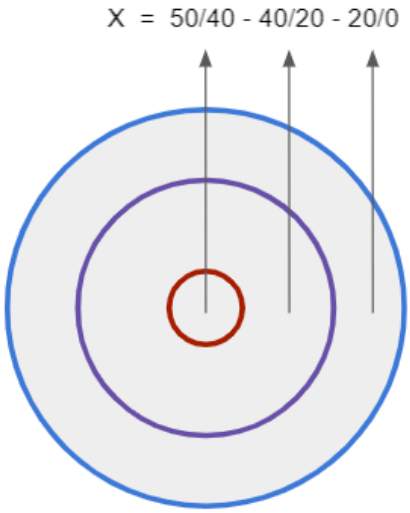

Figure 29: Division of the sample according to similarities in growth condition and thus in crystal shape. Areas as defined as: center, in-between and edge. X position varies from 0.000 (exactly in the edge - blue line) to 50.000 (exactly in the middle - center of red circle) with fixed Y=0.000.

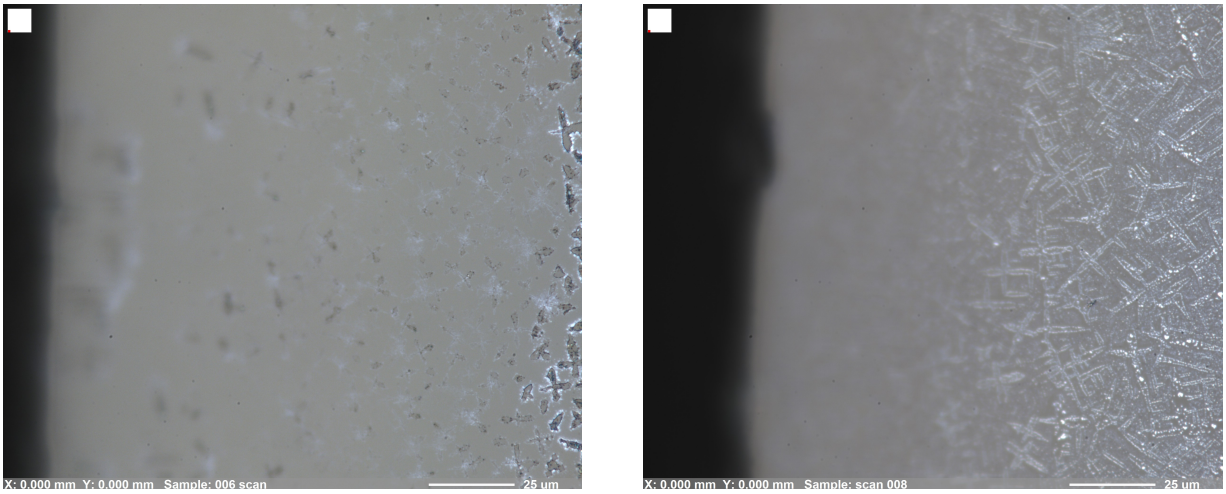

(a) Sample no 6. The black contrast around the crystals indicate the possibility of contamination.

(b) Sample no 8.

Figure 30: Analysis of the border of different samples to see the state of cleanness of the reactor - exactly the same growth conditions for both samples, the only difference is in reactor state. Image is de-focused because near the edges there is a significant curvature on the samples. Note to X:0.000 and Y:0.000 which indicates the (0,0) coordinates of which figure.

In Figure 30 it's possible to state the cleanliness of the reactor due to contamination. As stated, this contamination inhibits crystal growth and since the intention of the work is to create few atoms thick layer, any sort of contamination can have a big impact in the sample. Usually, it is desirable that this kind of reactors to be in an extremely clean environment, exactly to reduce the possibility of sample contamination.

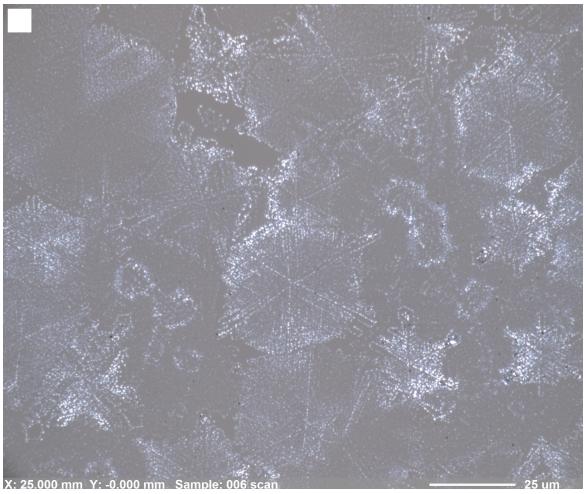

(a) Sample no 6. at X=25.000, note to dendritic shapes which indicate very small crystal lateral growth but big nucleation density.

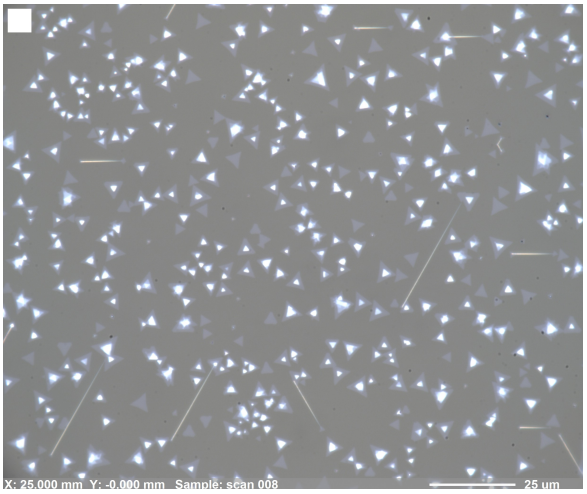

(b) Sample no 8. at X=25.000 crystals considerable bigger, with some mono layers (black triangle) and multi layers (bright triangle).

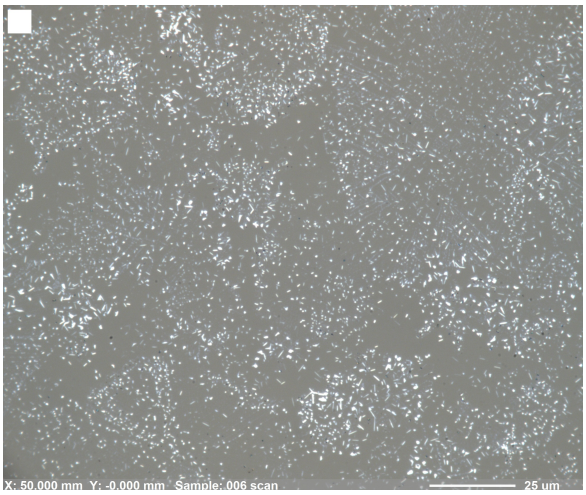

(c) Sample no 6. at X=50.000 with dendtric shape but with very bright small triangles indicating that it is mostly multi layer.

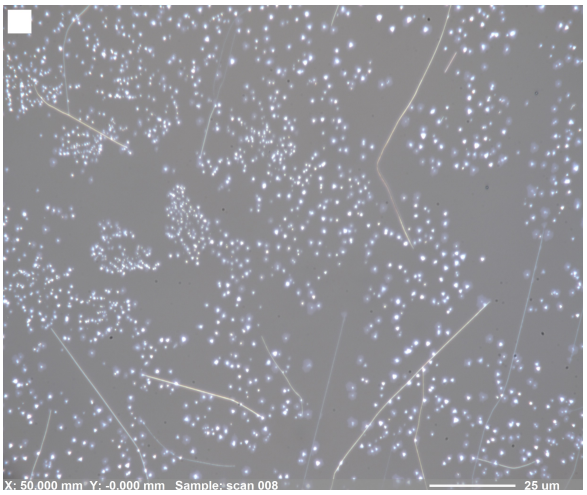

(d) Sample no 8. at X=50.000 with considerable smaller triangles and a lot of bright spots.

Figure 31: Effect on crystal size and quality according to state of cleanness inside the reactor.

Figure 31 points out a test which was done using water to achieve a cleaner state of the reactor - and it does has a big impact in crystal quality, at X=25.000 in sample 8 the mean crystal size is $8\mu m$, whereas in the same area of sample 6 crystal lateral size is smaller than $1\mu m$. In Figure 31b is possible to perceive a few triangles with multi layer, from that the gas flow was increased in order to form more mono layer crystals. Sample no. 9 and 10. have the same flow rate or H_2S (from x sscm to $x + 10$), the idea was also to visualize the importance to bake after every CVD and compare crystal size.

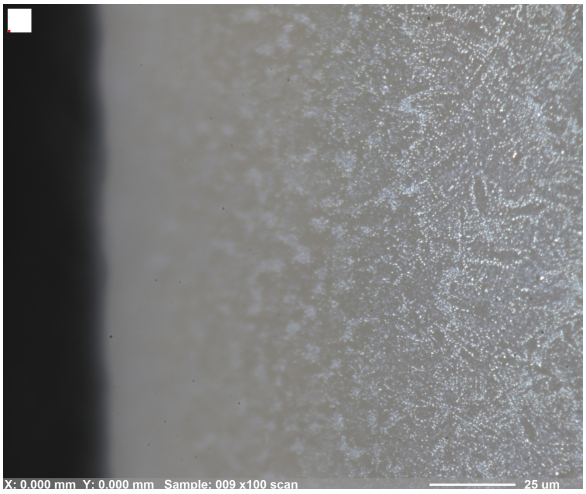

(a) Sample no 9. at X=0.000, no carbon contamination indication.

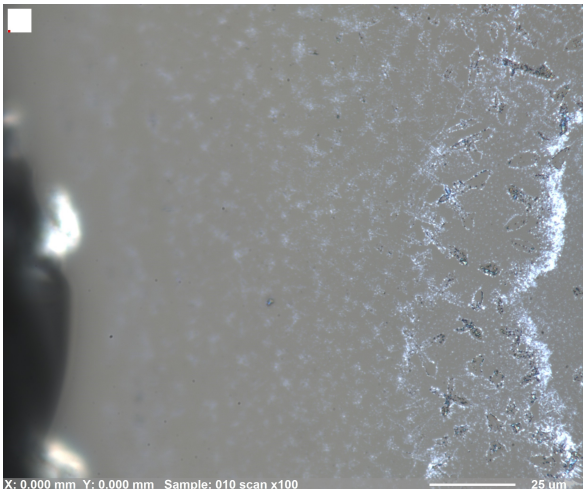

(b) Sample no 10. the black areas indicate contamination.

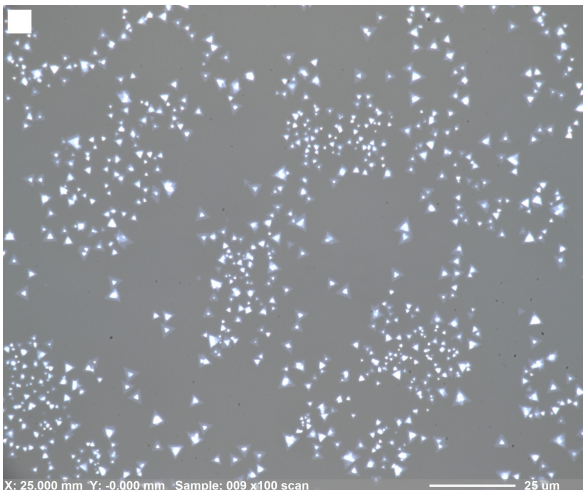

(c) Sample no 9. at X=25.000 some small triangles appear , but not as big as from sample no 8.

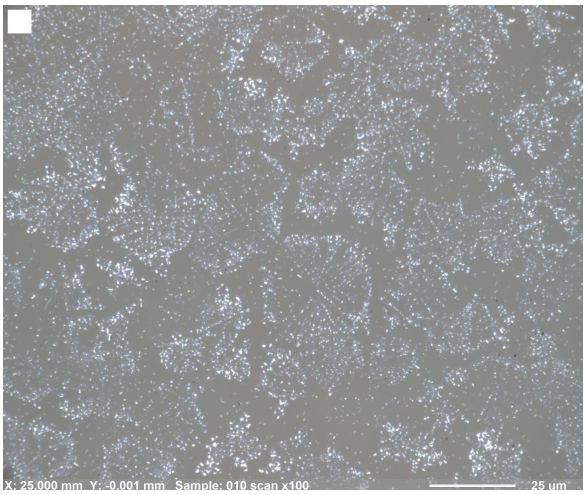

(d) Sample no 10. at X=25.000 with dendritic like shape.

Figure 32: Effect on crystal size and quality with a small increase of H_2S and reactor state after bake.

From Figure 32 is possible to perceive the importance of baking after every single CVD, a very clean reactor greatly affects the quality of the crystal, not only that, it also indicates that this contamination come from the gas line itself, rather than a possible external source. During growth the reactor is closed and there has been no other change between experiment no 9 and 10, which indicates that the sources comes from within the reactor, probably due to residual $Mo(CO)_6$ which is an attached pipeline that other users use, and some residual of this gas deposited inside the reactor. It's also possible to perceive that sample no 8 and sample no 9 are very similar in crystal size and quality, even suggesting that a lower H_2S flow might indicate bigger crystals, in this context both samples were more carefully analyzed using Fiji software.

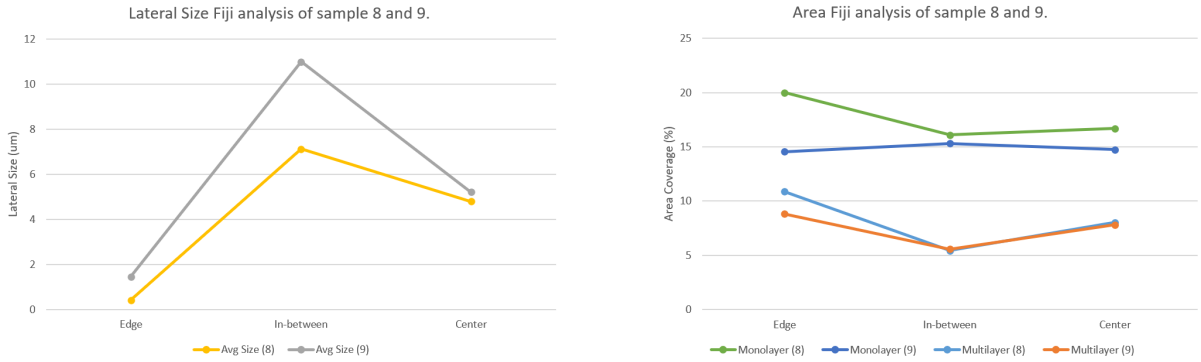

(a) Comparison between lateral size growth.

(b) Comparison between area growth.

Figure 33: Fiji analysis between sample no8 and no 9.

Figure 33 summarizes the analysis of many different optical microscope images of sample 8 to 9, from very close to the border all the way to the middle of the sample. As discussed in section 3.2.1 the smaller the crystal size the more imprecise it is to use contrast software to analyze the data. All measurements to calculate the covered area used the same sorting algorithm (Huang).

Firstly it's possible to observe that the covered area on samples 8 and 9 follow extremely similar trends, with generally sample no 8 having more area coverage, especially close to the edge, but since the crystal size is very small (smaller than $1\mu m$) there is little to no interest in this project. Multi layer coverage also has the same tendency with little to no deviance between both samples. Crystal average size in close to the edge and the center are very similar between both samples, but in the zone "in-between" (refer to image 29) crystal size between sample 8 and 9 show a big difference (almost 2 times of size difference), hence showing that a slight increase in the flow of H_2S has a slight impact on crystal size.

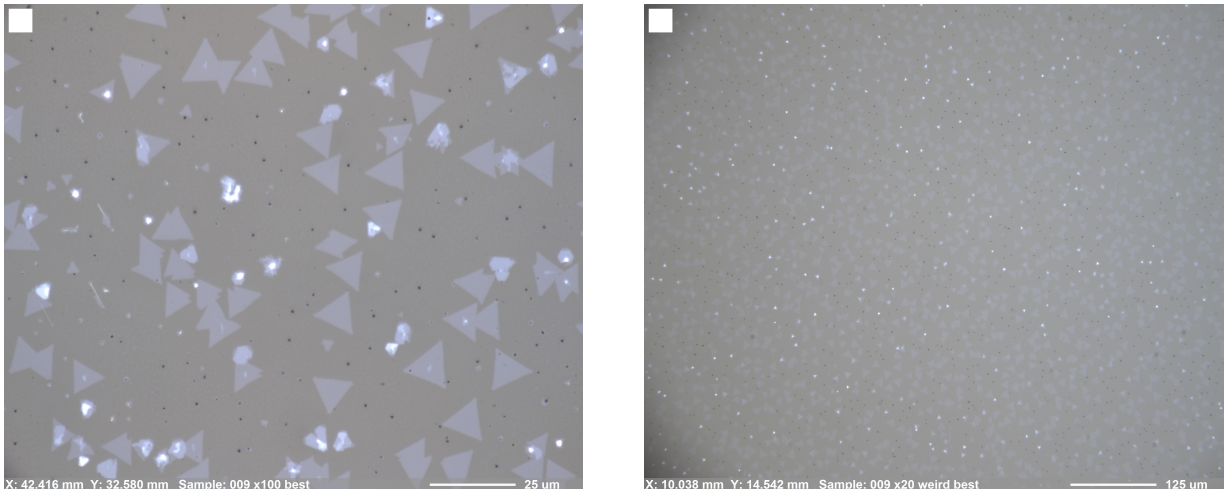

(a) Sample no 9. with x100 magnification, note to (x,y) position which puts in the same concentric circle as "in-between" area. It appears to have a numerous small black dots near to crystals, which hasn't appeared anywhere else in the sample.

(b) no 9. with x20 magnification average size is equal to 43 μm (which gives 14.3 μm lateral size). (x,y) position has no meaning since the sample has been moved due to small size of microscope, but it is geometrically close to figure a).

Figure 34: Analysis of the sample no9 showing big triangles proper for device fabrication.

Figure 34 shows the best area growth on sample no9 which was later used for device fabrication, although

this area is located in the "in-between" zone, those big crystals were only found in the upper part of the sample and not anywhere else, this might be due to inhomogeneity of gas flow inside the reactor. Also, this is the only area where it appears "black dots" which were later analyzed in SEM/EDX/AFM. This sample has shown 22.74% area coverage of MoS_2 material and 0.87% of multi-layer coverage, it also shows the same triangle orientation distribution as mentioned in the Figure 16, with high peaks of triangle oriented in 0 and 60 direction, and some minor peaks in 30 and 90 direction.

As mentioned there has been grown on Tube Furnace as well, there has been only one growth at this reactor and it has been done at 17/05/2021. Firstly, the concentration of Mo in liquid precursor is considerably higher than in Aixtron reactor (6 times higher), and there is the use of a hexacarbonyl precursor to supply the needed Mo, which also gradually increases during reaction time to fuel the reaction. Flow of H_2 are considerably smaller compared to Aixtron , temperature is 60 degrees smaller than Aixtron which greatly affect the electronic properties of the material, and tube furnace uses DES (Dimethyl sulfide) instead of H_2S.

In Figure 35 it's possible to observe the optical microscope image of tube furnace sample, this material has been grown several times in Lanes Laboratory using this furnace, so the recipe is very well established and thus giving a lot of monolayer coverage (due to past experiences done inside the lab proving that it's monolayer).

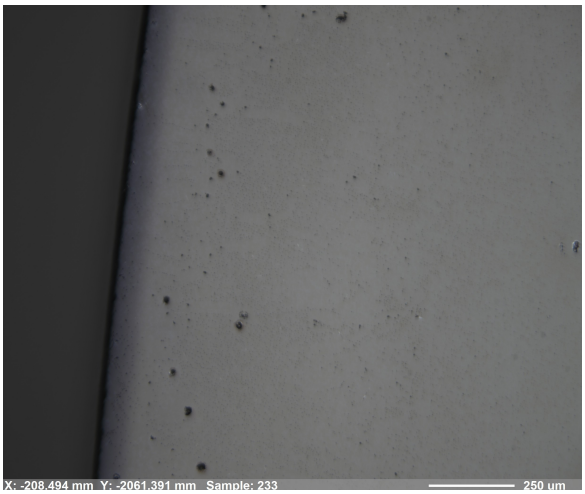

(a) Tube sample near the edge with x10 magnification, what is possible to observe here is full coverage of MoS_2.

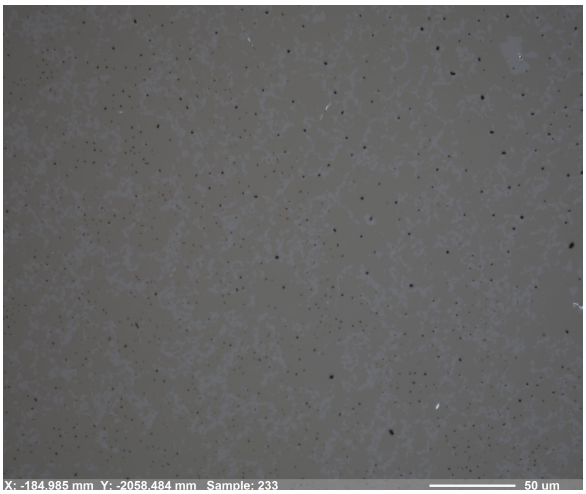

(b) Tube sample in the center with x50 magnification, mostly mono layer coverage, the brighter shapes are bi layer material. Note to black dots which also appear in this sample.

Figure 35: Optical Microscope of Tube Furnace sample.

Figure 36 shows an optical microscope image of Transferred Sample using the technique described in section 3.3.1. Figure a) shows the edge of the chips with all of it's markers, the purple area is the successful transferred MoS_2, figure b) shows the crystals in a SiO_2 substrate, on the edges of the figure it's possible to perceive the binary markers (in order to precisely identify the area of the sample), also some crystals are shattered this is due to the transfer procedure which applies a lot of stress on the triangles.

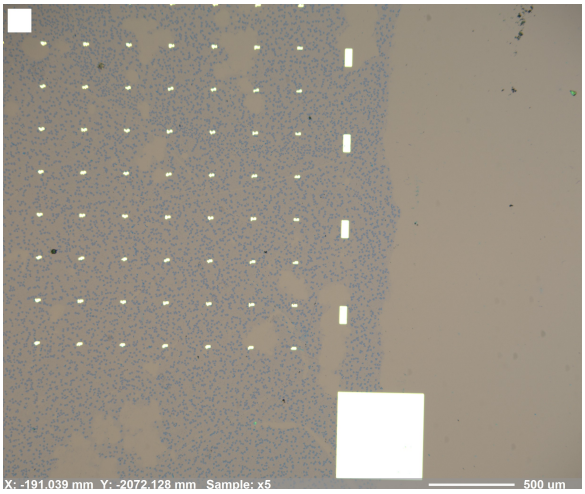

(a) Transferred MoS_2 sample no 9 from Aixtron at x5 magnification .

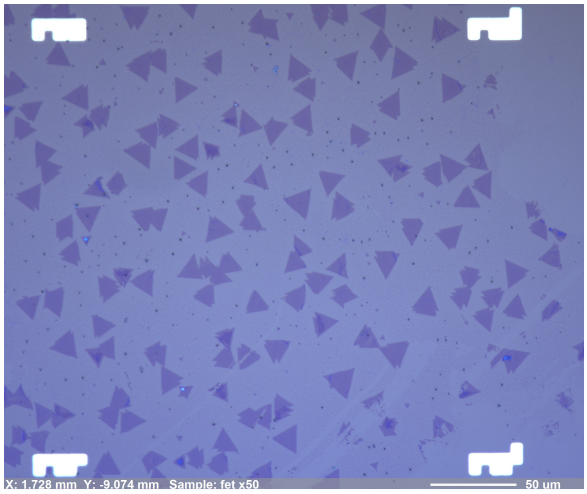

(b) Transferred MoS_2 sample no 9 from Aixtron at x50 magnification, note to the transfer of black balls as well.

Figure 36: Optical Microscope of Transferred Sample.

4.1.2 Scanning Electron Microscope & Energy Dispersive X-ray Spectroscopy

As mentioned in Section 3.2.2 and 3.2.3 SEM and EDX don't give the best results due to low signal to noise ratio of the sample, nonetheless it has proved useful for understanding the sample.

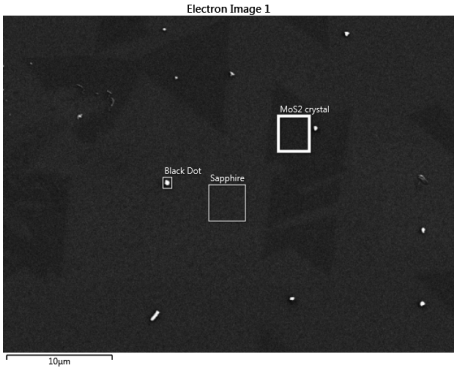

(a) SEM of Sample no 9, the white outlines represent the acquired area for EDX analysis in figure b . Black dots here are very bright white dots because of high electron reflection in comparison with other other elements.

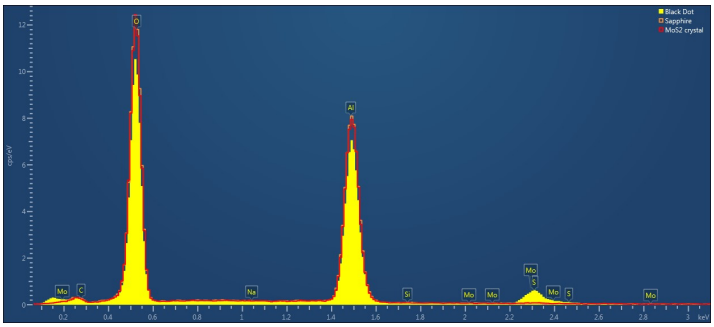

(b) EDX of Sample no 9, yellow spectra represents those of black dots, red and orange outlines represent MoS_2 crystal and Sapphire respectively.

Figure 37: SEM and EDX of Sample no 9.

Figure 37 shows the spectra obtained from sample no 9, as it's possible to observe on the EDX spectra, the "black dot" which was thought to be a carbon contamination which came from within the reactor actually is a complex of MoS_2 with high atomic %. The MoS_2 crystal and Sapphire are almost indistinguishable, only in figure 38 it's possible to perceive a small peak from the crystal, but not enough to point out a as a proof of deposition.

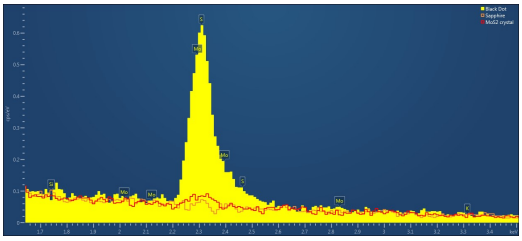

Figure 38: Close EDX Spectra from figure 37b with energy range from 1.7 to 3.4 keV.

As mentioned before, the EDX is also capable to give the atomic percentage of elements from the obtained spectra, and although the results are not coherent with this work, it's relevant to present them. C is considered in the spectra so that to observe possible carbon contamination on the sample, Na because the precursor of Mo is Na_2MoO_4, Si because EDX is a Si coating machine due to high use of other users and K because the Sapphire receive a KOH treatment.

In table 1 it's possible to observe the atomic percentage of EDX, there are a few results that stand out and some of them, as mentioned, it's not coherent to what it's observed in reality, first of all the MoS_2 crystal doesn't have stoichiometric Mo/S ratio and Sapphire has negative Na and S. The possible explanations to this incoherence are due to the fact that Sapphire is not a conductive substrate and the crystal is very thin and hardly perceived by the EDX, another possible argument is the low spectral resolution of measurement and small iteration numbers which is related to signal to noise ratio. Nonetheless it appears that there is still a considerable trace of carbon in the sample, which greatly reduce grain lateral growth. The alkaline metals are still residual (although on very low concentration) which might prone MoS_2 to doping.

Area/Element	C	O	Na	Al	Si	S	K	Mo	Total
Black Dot	1.68	53.28	0.10	37.46	0.13	4.22	0.19	2.95	100.00
MoS_2 crystal	0.98	55.81	0.07	42.43	0.01	0.29	0.17	0.25	100.00
Sapphire	0.80	56.19	-0.01	42.50	0.11	-0.06	0.26	0.22	100.00

Table 1: Atomic percentage from EDX spectra of sample no 9.

4.1.3 Atomic Force Microscope

AFM gives thickness information on the grown material, even more so than SEM/EDX due to the fact that it can image non conductive substrates.

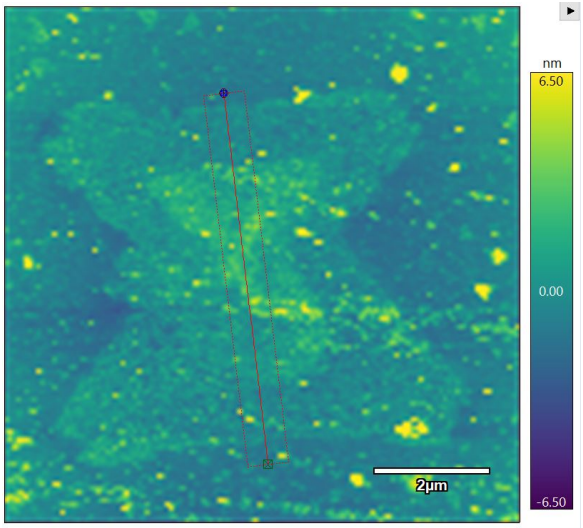

(a) Height trace plot of sample of multi layer crystal from sample no 9.

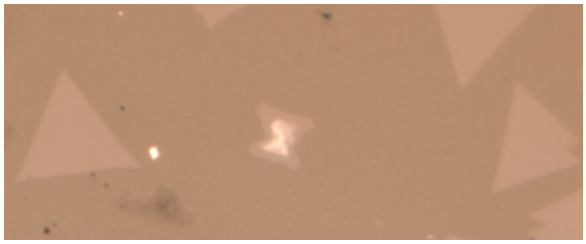

(b) Optical Microscope Image of given area, note to bright triangles inside which indicate multi layer area.

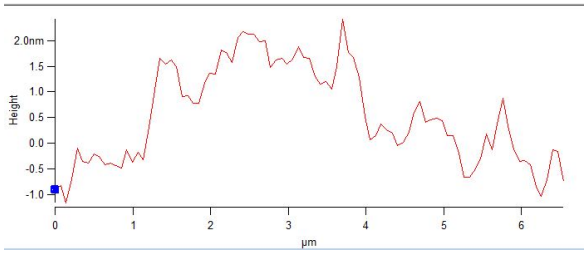

(c) Height trace of the black line in figure a). Blue dot indicate the beginning of the trace.

Figure 39: AFM of Sample no 9 on Sapphire indicating mono layer and multi layer.

In Figure 39 it's possible to observe the height of a monolayer and multi layer areas, when x = [0,1] defines the monolayer area which gives close to 0,75 nm of height, when x =[1.5,5] enters the multi layer area with varying height from 1.5 nm to 4.5 nm, when x = [5,6.5] the probe enter on a dirty mono layer region, with expected height of 0.75 nm and some peaks of up to 2.5 nm. This dirtiness comes from the fact that is necessary to dice the Sapphire sample into very small areas, thus cracking the sample and bits of particle deposing on the surface.

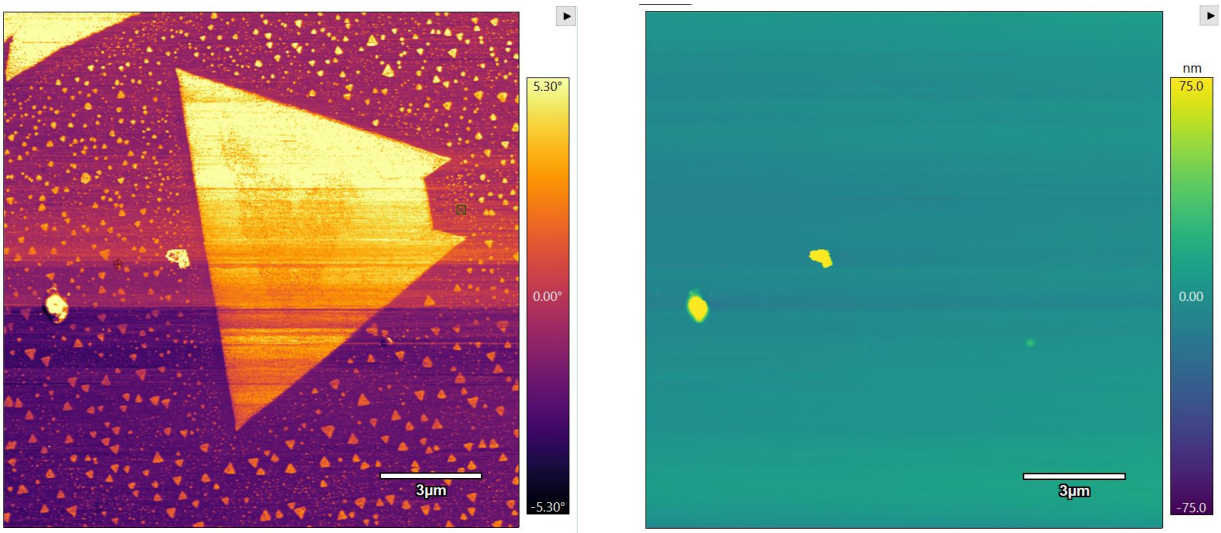

(a) Phase trace plot of the sample, note to very small epitaxial (0°and 60°orientation) the yellow clusters are the "black balls".

(b) Height trace plot of the sample, the height of the crystals are hard to observe due to high heights of the "black balls".

Figure 40: AFM of Sample no 9 on Sapphire.

In figure 40 it's possible to observe a AFM scan of sample no 9, in figure a) most of the crystals are epitaxial, and in figure b) it's possible to observe the high height of the black balls (close to 75 nm) compared to a mono layer from previous figure which is 0,75 nm.

4.1.4 Photoluminescence

In Figure 41 shows the photoluminescence of different MoS_2 samples, blue line from grown on Aixtron (sample no 8) with PL peak at 1.87 eV, orange line from Tube Furnace with PL peak at 1.84 eV and green line Transferred on SiO_2 with PL peak at 1.85 eV. Firstly, the A Exciton peak from Aixtron is 32 meV higher than the one from Tube Furnace, this may be due to different growth temperature (at least 150°C higher in Aixtron) which induces a larger lattice strain between the deposited material and the substrate and therefore slightly changing the energy of band gap [40]. This is proven again when compares the band gap of the Transferred Sample with Tube Furnace, there is a 13 meV difference, which indicates the gaps are closer and SiO_2 sample has less strain since the transfer process removes all the strain with the substrate.

There is a small Sapphire peak in the Aixtron curve, which comes from the fact that the intensity is enough for the peak to manifest itself (much stronger signal might suppress this result in the curve, which happens on the Tube Furnace curve - this happens because the area coverage of this sample is way bigger, thus resulting in a stronger PL). The B exciton only appears in the SiO_2 because the the strain in the sample is close to none, which permits the manifestation of this energy peak.

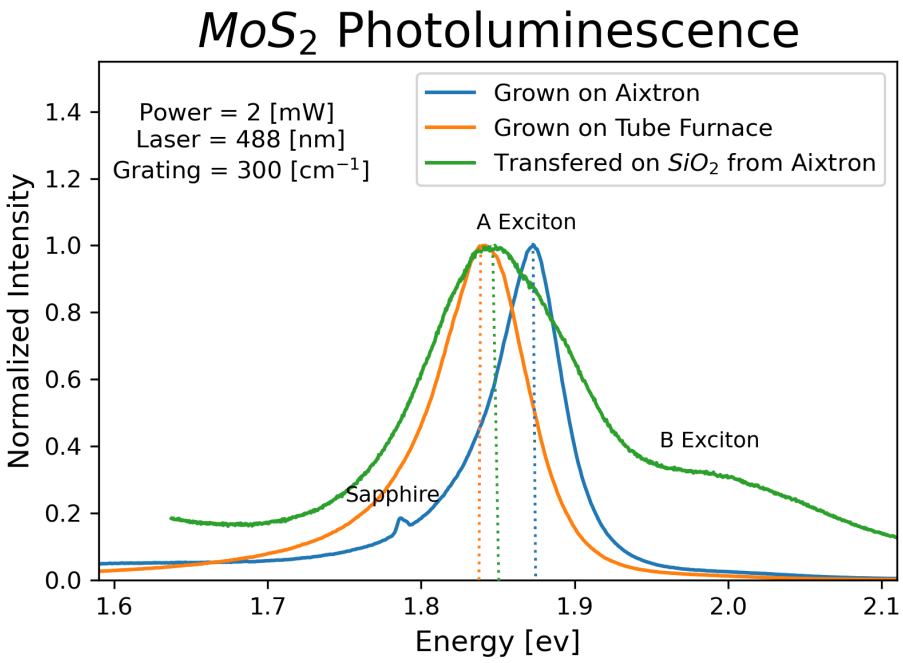

Figure 41: MoS_2 Photoluminescence of different types of sample, dashed lines show the peak energy position.

4.1.5 Raman Spectroscopy

As discussed in section 3.2.6 Raman Spectroscopy is a frequently used tool in 2D material analysis due to capacity to observe if there is monolayer or multi layer based on the distance between the excitation peaks. In Figure 42 the separation between E^1_{2G} and A_{1G} peaks of mono layer and multi layer are respectively 22.48 cm^{-1} and 25.69 cm^{-1} which is fairly similar with reference [42] which gives 21.8 cm^{-1} for monolayer and 25.1 cm^{-1} to multi layer.

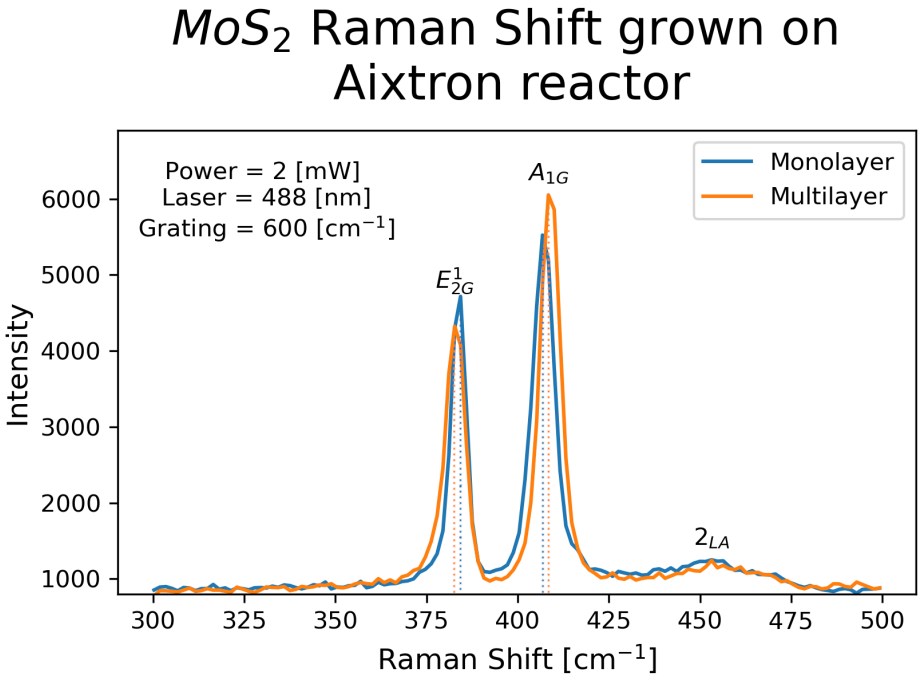

Figure 42: MoS_2 Raman Shift of mono layer and multi layer.

Figure 43 shows the Raman spectra obtained from Aixtron reactor, Tube Furnace and Transferred Sample. Firstly it' s possible to perceive that E^1_{2G} peaks Raman shift are almost the same, with a small difference of 0.4 cm^{-1} on Transferred sample. On the other side A_{1G} Raman shift peak position are precisely the same for Tube Furnace and SiO_2 which indicates that it's stress related peak since the transfer to SiO_2 releases all the stress from substrate and deposited material [40].

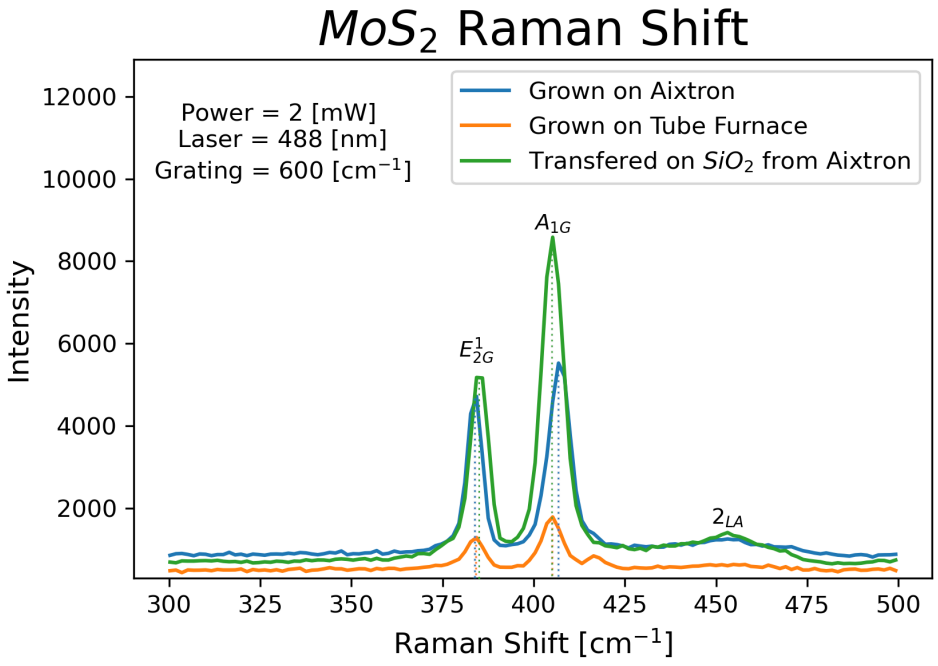

Figure 43: MoS_2 Raman Shift of Aixtron, Tube Furnace and Transferred Sample.

4.2 Electrical properties

In this section the electrical properties of the material have been discussed and analyzed. Figure 44a-c shows the CAD, exposed and final device figures of MoS_2 FET.

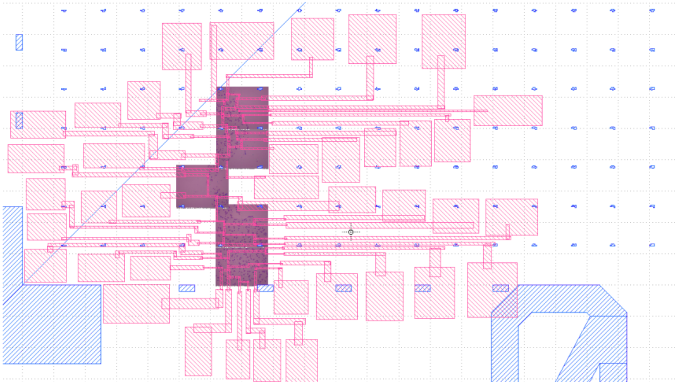

(a) CAD File and patterns for laser writing.

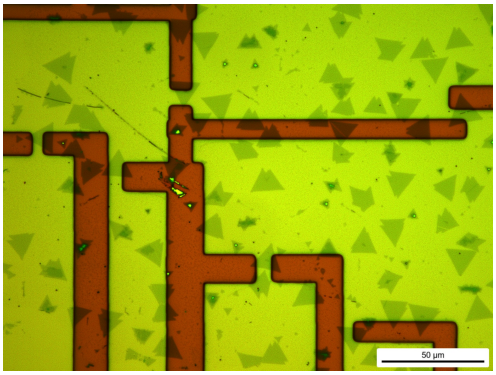

(b) Exposed material, just before metal deposition.

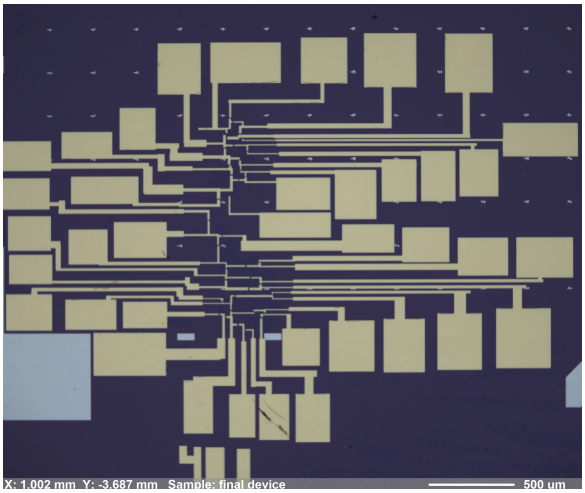

(c) Final device after metal deposition and lift-off.

Figure 44: CAD, exposed and final device figures.

4.2.1 Transfer characteristics

The characterization of transistors looks into their current response according to a sweep voltage, in the case of transfer characteristics, the observed result is the current flown from drain to source in response to varying gate voltage.

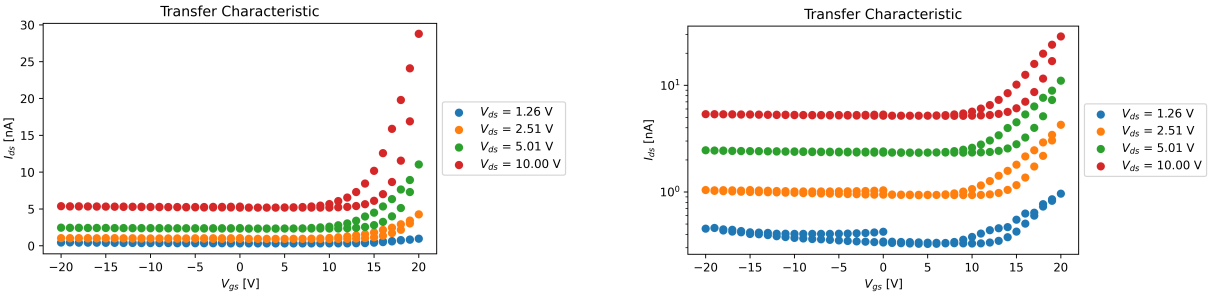

(a) Transfer Characteristics with varying voltage on a linear scale.

(b) Transfer Characteristics with varying voltage on a log scale.

Figure 45: Transfer Characteristic Curves.

In figure 45 it's possible to observe the described experiment, which gives relevant information about the device made, for instance, with high positive gate voltage there is a high peak of current which indicates a n type transistor. According to Dolui [43], the origin of the n-type of MoS2 monolayers on a SiO2 substrate is due to trapped charges at the SiO2 and can also be related to intrinsic sulfur vacancies in monolayer MoS_2 [44].

When Vg is negative (specially at lower Vds) the material also conducts, which indicates that it has an ambivalent property (there is also hole conduction), this argument is further sustained because Ig vs Vg curves (Figure 46a) aren't symmetric to the transfer curves, this is due to IOFF current increasing as a function of the increase on Vds which indicates Hopping transport (due to defects) [45]. This could be better explored if wider sweep of Vds sweep was done without applying a positive. The p type behavior is probably due to oxidization due to air exposure and throughout the fabrication process.

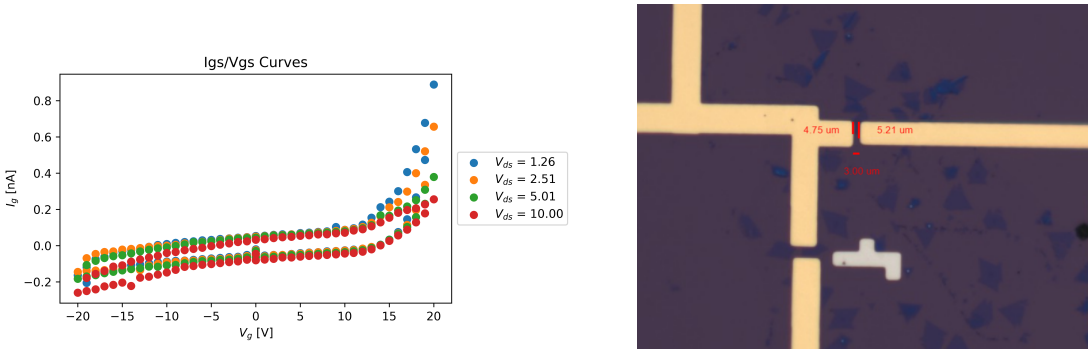

(a) TI_g /V_g curve.

(b) Geometry of channel.

Figure 46: I_g /V_g curve and geometry of channel.

Curve 45 also present a hysteresis effect which is observed when the Vg is increased, because it presents a different current from when Vg is decreased. According to Jiapei Shu et al [46] this is due to charge redistribution under the gate voltage, including charge transfer, charge trapping or charge polarization.It is then reasonable that there are charges in the MoS2 channel that can be redistributed by the strong external electric field.

The geometry of the MoS_2 channel is shown in Figure 46b, in which the channel length, left width, and right width are respectively 3.00 µm, 4.75 µm, 5.21 µm and thus the L/W can be calculated as:

$$w = W_1 + \frac{(W_2 - W_1)}{L}\, l = 4.75 + 0.153\, l \tag{20}$$

$$\frac{L}{W} = \int_0^3 \frac{l}{4.75 + 0.153\, l} dl = 0.663 \tag{21}$$

The capacitance of SiO_2 can be calculated accordingly:

$$C_{SiO_2} = \frac{\epsilon_{ox}}{t_{ox}} = \frac{3.415\ 10^{-13}}{270\ 10^{-9}} = 1.27\ 10^{-6} F/cm^{-2} \tag{22}$$

From the Ids-Vds curve is also possible to obtain the slope of the curve $\delta(I_{ds}/V_{ds})$. The field effect mobility is represented in Figure 47 and can be obtained by:

$$\mu_{eff} = \frac{\delta(I_{ds})}{\delta(V_{gs})} \frac{L}{W} \frac{1}{V_{ds}} \frac{1}{C_{SiO_2}} \tag{23}$$

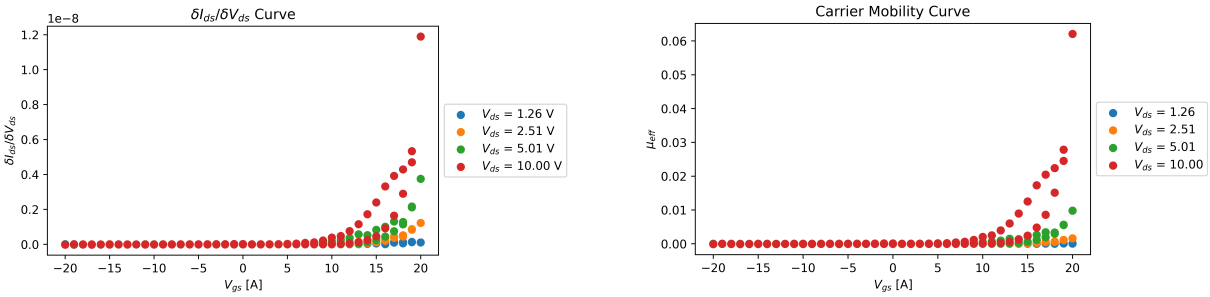

(a) Slope of transfer curve.

(b) Effectivity mobility.

Figure 47: Slope and carrier mobility curves.

The low mobility can be explained according to degradation of crystal by oxidation because this sample was not kept in glove box, and also degradation during fabrication process.

With curve from Figure 45 is also possible to obtain the threshold voltage with linear extrapolation method, where the linear part of Figure 45a is extrapolated at $y = 0$ and the x value gives the threshold voltage. In this scenario the threshold voltages are between to 3 to 4 Volts.

4.2.2 Output Characteristics

Output Characteristics also known as I-V curves are one of the most common methods of determining how an electrical device functions in a circuit. It consists on applying a varying V_{ds} voltage and registering the current obtained. With this type of measurement it's possible to determine the type of contact that this device applies in an electrical circuit.

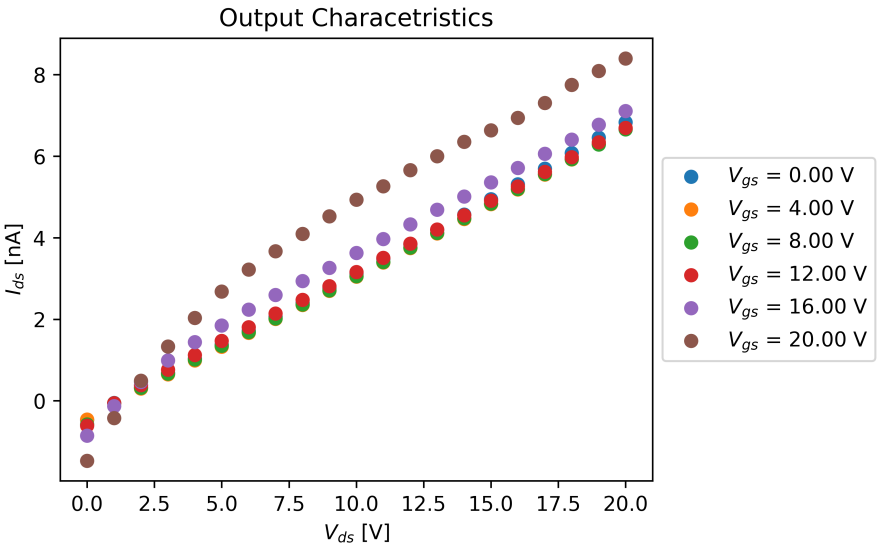

Figure 48: Output Characteristics Curve

In figure 48 it's possible to observe the output characteristics of MoS_2, for low gate voltages ($V_g = 0V$ the MoS_2 presents a linear behavior across the whole V_{ds} sweep, but with higher drain scource voltage, for example $V_g = 20V$ the FET device loses its linearity and enters a saturation regime at about Vds = 10V.

5 Conclusion

This project that has been done during the 6 month internship at EPFL been fruitful for my formation, I took numerous training courses in white rooms to learn how to handle equipment, I handled growth, manufacturing and characterization machines. The work was essentially practical, and looking back on the numerous aspects covered it is safe to say that the work here done has successfully accomplished it's goal, which is basically consisted in manufacturing a MoS_2 device using a showerhead system.

The first part of the work, which consisted of CVD growth, was based by articles and books on the subject, giving special focus to CVD of MoS_2. Several types of growth were discussed, it was elucidated how to grow this material in this internship, giving the necessary theoretical background for each part of the process. In addition to the necessary theoretical background, growth results varying in some parameters were also presented - emphasizing in particular the need for a clean reactor.

The second part of this work consisted in characterizing the grown material, which despite not being something demanded by the internship proposal, the grown material was characterized in several ways, both in order to better understand its behavior and to understand problems that could occur during growth. All these techniques were properly explained, giving a sufficient theoretical basis for the understanding of the results. Besides the fundamentals, the parameters used were also given, so that people can later reproduce these same experiments without having to go through the arduous task of trial and error until the best parameter is found. Besides all this background, AFM, EDX, SEM, OM, Raman results were presented and discussed.

The third part of this work consisted of manufacturing the device, in which the necessary routine for manufacturing was also given, besides briefly discussing the why of each step. In addition, the workflow used was also presented in the Appendix so that it can be used later by other people in the group. Different fabrication results were also presented, emphasizing in particular the most delicate step which was the transfer of the material MoS_2 to a silicon chip.

The last step was to present the results of the characterization of the FET produced. In a first moment, it was explained what a FET was about through its band diagrams. In a second moment, the equations used to obtain its properties were explained, and finally the results obtained were presented. All the results were also discussed accordingly, and are satisfactory for the objective of the internship.

Finally, a long work that satisfactorily approaches the fabrication of MoS_2 devices and fulfills the main objective of the work, which is to train the student to later work in something more innovative in the area. Personally, I am happy with what was possible to do in the work and I am sure that this learning will help a lot in my formation as an engineer.

References

[1] Ossila, "Molybdenum disulfide (mos2):theory applications." https://www.ossila.com/pages/molybdenum-disulfide-mos2, May 2021.

[2] A. e. a. Splendiani, "Emerging photoluminescence in monolayer mos2," *Nano Lett.*, vol. 4, p. 4041, 04 2010.

[3] K. F. Mak, C. Lee, J. Hone, J. Shan, and T. F. Heinz, "Atomically thin mos2: A new direct-gap semiconductor," *Phys. Rev. Lett.*, vol. 105, p. 136805, Sep 2010.

[4] D. Xiao, G.-B. Liu, W. Feng, X. Xu, and W. Yao, "Coupled spin and valley physics in monolayers of mos_2 and other group-vi dichalcogenides," *Phys. Rev. Lett.*, vol. 108, p. 196802, May 2012.

[5] K. F. Mak, D. Xiao, and J. Shan, "Light–valley interactions in 2D semiconductors," *Nature Photonics 2018 12:8*, vol. 12, pp. 451–460, jul 2018.

[6] G. Wang, A. Chernikov, M. M. Glazov, T. F. Heinz, X. Marie, T. Amand, and B. Urbaszek, "Colloquium: Excitons in atomically thin transition metal dichalcogenides," *Reviews of Modern Physics*, vol. 90, p. 021001, apr 2018.

[7] A. Chernikov, T. C. Berkelbach, H. M. Hill, A. Rigosi, Y. Li, O. B. Aslan, D. R. Reichman, M. S. Hybertsen, and T. F. Heinz, "Exciton Binding Energy and Nonhydrogenic Rydberg Series in Monolayer WS 2," 2014.

[8] A. Ciarrocchi, "Electronic, excitonic and magnetic properties of two-dimensional heterostructures," 2020. EPFL, 10.5075/EPFL-THESIS-8443.

[9] H.-M. e. a. Li, "Metal-semiconductor barrier modulation for high photoresponse in transition metal dichalcogenide field effect transistors," *Scientific Reports*, vol. 4, p. 4041, 02 2014.

[10] *Thermodynamics and Kinetics of Chemical Vapour Deposition*, pp. 129–164. London: Springer London, 2010.

[11] D. Dumcenco, D. Ovchinnikov, K. Marinov, P. Lazić, M. Gibertini, N. Marzari, O. L. Sanchez, Y.-C. Kung, D. Krasnozhon, M.-W. Chen, S. Bertolazzi, P. Gillet, A. Fontcuberta i Morral, A. Radenovic, and A. Kis, "Large-Area Epitaxial Monolayer MoS2," *ACS Nano*, vol. 9, pp. 4611–4620, Apr. 2015. Publisher: American Chemical Society.

[12] S. Boandoh, S. H. Choi, J.-H. Park, S. Y. Park, S. Bang, M. S. Jeong, J. S. Lee, H. J. Kim, W. Yang, J.-Y. Choi, S. M. Kim, and K. K. Kim, "A Novel and Facile Route to Synthesize Atomic-Layered MoS2 Film for Large-Area Electronics," *Small*, vol. 13, no. 39, p. 1701306, 2017. _eprint: https://onlinelibrary.wiley.com/doi/pdf/10.1002/smll.201701306.

[13] H. Kim, D. Ovchinnikov, D. Deiana, D. Unuchek, and A. Kis, "Suppressing Nucleation in Metal–Organic Chemical Vapor Deposition of MoS $_2$ Monolayers by Alkali Metal Halides," *Nano Letters*, vol. 17, pp. 5056–5063, Aug. 2017.

[14] A. Molina-Sánchez and L. Wirtz, "Phonons in single-layer and few-layer mos_2 and ws_2," *Phys. Rev. B*, vol. 84, p. 155413, Oct 2011.

[15] O. V. Yazyev and A. Kis, "MoS2 and semiconductors in the flatland," *Materials Today*, vol. 18, pp. 20–30, Jan. 2015.

[16] D. Lembke, S. Bertolazzi, and A. Kis, "Single-Layer MoS2 Electronics," *Accounts of Chemical Research*, vol. 48, pp. 100–110, Jan. 2015. Publisher: American Chemical Society.

[17] K.-K. Liu, W. Zhang, Y.-H. Lee, Y.-C. Lin, M.-T. Chang, C.-Y. Su, C.-S. Chang, H. Li, Y. Shi, H. Zhang, C.-S. Lai, and L.-J. Li, "Growth of Large-Area and Highly Crystalline MoS2 Thin Layers on Insulating Substrates," *Nano Letters*, vol. 12, pp. 1538–1544, Mar. 2012. Publisher: American Chemical Society.

[18] M. Seol, M.-H. Lee, H. Kim, K. W. Shin, Y. Cho, I. Jeon, M. Jeong, H.-I. Lee, J. Park, and H.-J. Shin, "High-throughput growth of wafer-scale monolayer transition metal dichalcogenide via vertical ostwald ripening," *Advanced Materials*, vol. 32, no. 42, p. 2003542, 2020.

[19] D. Unuchek, *Spin-valley optoelectronics based on two-dimensional materials*. PhD thesis, 2019. EPFL, 10.5075/EPFL-THESIS-7473.

[20] Y. ZHAO, *Electronic Properties of Synthetic 2D Materials*. 2018. EPFL.

[21] H. Pierson, *Handbook of Chemical Vapor Depostion [i.e. Deposition] (CVD): Principles, Technology, and Applications*. Chemical, Petrochemical & Process, Noyes Publications/William Andrew Pub., 1999.

[22] S. D. Hersee and J. M. Ballingall, "The operation of metalorganic bubblers at reduced pressure," *Journal of Vacuum Science & Technology A*, vol. 8, no. 2, pp. 800–804, 1990.

[23] W. Chen, J. Zhao, J. Zhang, L. Gu, Z. Yang, X. Li, H. Yu, X. Zhu, R. Yang, D. Shi, X. Lin, J. Guo, X. Bai, and G. Zhang, "Oxygen-Assisted Chemical Vapor Deposition Growth of Large Single-Crystal and High-Quality Monolayer MoS2," *Journal of the American Chemical Society*, vol. 137, pp. 15632–15635, dec 2015.

[24] H. Pierson, *Handbook of Chemical Vapor Deposition, 2nd Edition: Principles, Technology and Applications*. Elsevier Science, 2013.

[25] D. Sengupta, S. Mazumder, W. Kuykendall, and S. A. Lowry, "Combined ab initio quantum chemistry and computational fluid dynamics calculations for prediction of gallium nitride growth," *Journal of Crystal Growth*, vol. 279, no. 3, pp. 369–382, 2005.

[26] H. Cun, M. Macha, H. Kim, K. Liu, Y. Zhao, T. LaGrange, A. Kis, and A. Radenovic, "Wafer-scale MOCVD growth of monolayer MoS2 on sapphire and SiO2," *Nano Research*, vol. 12, pp. 2646–2652, Oct. 2019.

[27] H. Kim, D. Dumcenco, M. Frégnaux, A. Benayad, M.-W. Chen, Y.-C. Kung, A. Kis, and O. Renault, "Free-standing electronic character of monolayer mos2 in van der Waals epitaxy," *Physical Review B*, vol. 94, p. 081401, Aug. 2016. Publisher: American Physical Society.

[28] A. A. Mitioglu, K. Galkowski, A. Surrente, L. Klopotowski, D. Dumcenco, A. Kis, D. K. Maude, and P. Plochocka, "Magnetoexcitons in large area CVD-grown monolayer mos2 and mose2 on sapphire," *Physical Review B*, vol. 93, p. 165412, Apr. 2016. Publisher: American Physical Society.

[29] M. Yoshimoto, T. Maeda, T. Ohnishi, H. Koinuma, O. Ishiyama, M. Shinohara, M. Kubo, R. Miura, and A. Miyamoto, "Atomic-scale formation of ultrasmooth surfaces on sapphire substrates for high-quality thin-film fabrication," *Applied Physics Letters*, vol. 67, pp. 2615–2617, Oct. 1995. Publisher: American Institute of Physics.

[30] Z. Ma, S. Wang, Q. Deng, Z. Hou, X. Zhou, X. Li, F. Cui, H. Si, T. Zhai, and H. Xu, "Epitaxial Growth of Rectangle Shape MoS2 with Highly Aligned Orientation on Twofold Symmetry a-Plane Sapphire," *Small*, vol. 16, no. 16, p. 2000596, 2020. _eprint: https://onlinelibrary.wiley.com/doi/pdf/10.1002/smll.202000596.

[31] H. Yu, Z. Yang, L. Du, J. Zhang, J. Shi, W. Chen, P. Chen, M. Liao, J. Zhao, J. Meng, G. Wang, J. Zhu, R. Yang, D. Shi, L. Gu, and G. Zhang, "Precisely Aligned Monolayer MoS2 Epitaxially Grown on h-BN basal Plane," *Small*, vol. 13, no. 7, p. 1603005, 2017. _eprint: https://onlinelibrary.wiley.com/doi/pdf/10.1002/smll.201603005.

[32] Z. Jin, S. Shin, D. Hyun Kwon, S.-J. Han, and Y.-S. Min, "Novel chemical route for atomic layer deposition of MoS 2 thin film on SiO 2 /Si substrate," *Nanoscale*, vol. 6, no. 23, pp. 14453–14458, 2014. Publisher: Royal Society of Chemistry.

[33] Y. Cheng, K. Yao, Y. Yang, L. Li, Y. Yao, Q. Wang, X. Zhang, Y. Han, and U. Schwingenschlögl, "Van der Waals epitaxial growth of MoS 2 on SiO 2 /Si by chemical vapor deposition," *RSC Advances*, vol. 3, no. 38, pp. 17287–17293, 2013. Publisher: Royal Society of Chemistry.

[34] C.-p. Tso, C.-m. Zhung, Y.-h. Shih, Y.-M. Tseng, S.-c. Wu, and R.-a. Doong, "Stability of metal oxide nanoparticles in aqueous solutions," *Water Science and Technology*, vol. 61, pp. 127–133, Jan. 2010.

[35] F. Ghasemi, R. Frisenda, D. Dumcenco, A. Kis, D. Perez de Lara, and A. Castellanos-Gomez, "High Throughput Characterization of Epitaxially Grown Single-Layer MoS2," *Electronics*, vol. 6, p. 28, June 2017. Number: 2 Publisher: Multidisciplinary Digital Publishing Institute.

[36] S. Manzeli, D. Ovchinnikov, D. Pasquier, O. V. Yazyev, and A. Kis, "2D transition metal dichalcogenides," *Nature Reviews Materials*, vol. 2, pp. 1–15, June 2017. Number: 8 Publisher: Nature Publishing Group.

[37] C. Backes, A. M. Abdelkader, C. Alonso, A. Andrieux-Ledier, R. Arenal, J. Azpeitia, N. Balakrishnan, L. Banszerus, J. Barjon, R. Bartali, S. Bellani, C. Berger, R. Berger, M. M. B. Ortega, C. Bernard, P. H. Beton, A. Beyer, A. Bianco, P. Bøggild, F. Bonaccorso, G. B. Barin, C. Botas, R. A. Bueno, D. Carriazo, A. Castellanos-Gomez, M. Christian, A. Ciesielski, T. Ciuk, M. T. Cole, J. Coleman, C. Coletti, L. Crema, H. Cun, D. Dasler, D. D. Fazio, N. Díez, S. Drieschner, G. S. Duesberg, R. Fasel, X. Feng, A. Fina, S. Forti, C. Galiotis, G. Garberoglio, J. M. García, J. A. Garrido, M. Gibertini, A. Gölzhäuser, J. Gómez, T. Greber, F. Hauke, A. Hemmi, I. Hernandez-Rodriguez, A. Hirsch, S. A. Hodge, Y. Huttel, P. U. Jepsen, I. Jimenez, U. Kaiser, T. Kaplas, H. Kim, A. Kis, K. Papagelis, K. Kostarelos, A. Krajewska, K. Lee, C. Li, H. Lipsanen, A. Liscio, M. R. Lohe, A. Loiseau, L. Lombardi, M. F. López, O. Martin, C. Martín, L. Martínez, J. A. Martin-Gago, J. I. Martínez, N. Marzari, Mayoral, J. McManus, M. Melucci, J. Méndez, C. Merino, P. Merino, A. P. Meyer, E. Miniussi, V. Miseikis, N. Mishra, V. Morandi, C. Munuera, R. Muñoz, H. Nolan, L. Ortolani, A. K. Ott, I. Palacio, V. Palermo, J. Parthenios, I. Pasternak, A. Patane, M. Prato, H. Prevost, V. Prudkovskiy, N. Pugno, T. Rojo, A. Rossi, P. Ruffieux, P. Samorì, L. Schué, E. Setijadi, T. Seyller, G. Speranza, C. Stampfer, I. Stenger, W. Strupinski, Y. Svirko, S. Taioli, K. B. K. Teo, M. Testi, F. Tomarchio, M. Tortello, E. Treossi, A. Turchanin, E. Vazquez, E. Villaro, P. R. Whelan, Z. Xia, R. Yakimova, S. Yang, G. R. Yazdi, C. Yim, D. Yoon, X. Zhang, X. Zhuang, L. Colombo, A. C. Ferrari, and M. Garcia-Hernandez, "Production and processing of graphene and related materials," *2D Materials*, vol. 7, p. 022001, Jan. 2020. Publisher: IOP Publishing.

[38] X. Li, X. Li, X. Zang, M. Zhu, Y. He, K. Wang, D. Xie, and H. Zhu, "Role of hydrogen in the chemical vapor deposition growth of MoS2 atomic layers," *Nanoscale*, vol. 7, pp. 8398–8404, Apr. 2015. Publisher: The Royal Society of Chemistry.

[39] A. R. an Oxford Instruments company, "Imaging and spectroscopy applications guide," 2016.

[40] P. C. Braga, *Calcul de propriétés physiques de semi-conducteurs III-V pour leur fabrication par MOVPE et leur caractérisationn.* 2020. Grenoble INP.

[41] H. Zobeiri, S. Xu, Y. Yue, Q. Zhang, Y. Xie, and X. Wang, "Effect of temperature on raman intensity of nm-thick ws2: Combined effects of resonance raman, optical properties, and interface optical interference," *Nanoscale*, vol. 12, 02 2020.

[42] S. Xiao, P. Xiao, X. Zhang, Y. Da-Wei, X. Gu, F. Qin, Z. Ni, Z. J. Han, and K. Ostrikov, "Atomic-layer soft plasma etching of mos2," *Scientific Reports*, vol. 6, p. 19945, 01 2016.

[43] K. Dolui, I. Rungger, and S. Sanvito, "Origin of then-type andp-type conductivity of mos2monolayers on a sio2substrate," *Physical Review B*, vol. 87, Apr 2013.

[44] J. Su, N. Li, Y. Zhang, L. Feng, and Z. Liu, "Role of vacancies in tuning the electronic properties of au-mos2 contact," *AIP Advances*, vol. 5, no. 7, p. 077182, 2015.

[45] D. Jariwala, V. K. Sangwan, D. J. Late, J. E. Johns, V. P. Dravid, T. J. Marks, L. J. Lauhon, and M. C. Hersam, "Band-like transport in high mobility unencapsulated single-layer mos2 transistors," *Applied Physics Letters*, vol. 102, no. 17, p. 173107, 2013.

[46] J. Shu, G. Wu, Y. Guo, B. Liu, X. Wei, and Q. Chen, "The intrinsic origin of hysteresis in mos2 field effect transistors," *Nanoscale*, vol. 8, pp. 3049–3056, 2016.

6 Appendix

This section is destined for information which is not crucial to the comprehension of the work done, but is relevant for those who are interested in the burocractis aspect of the work, especially those who may work in the future at Lanes lab.

6.1 Gantt Chart

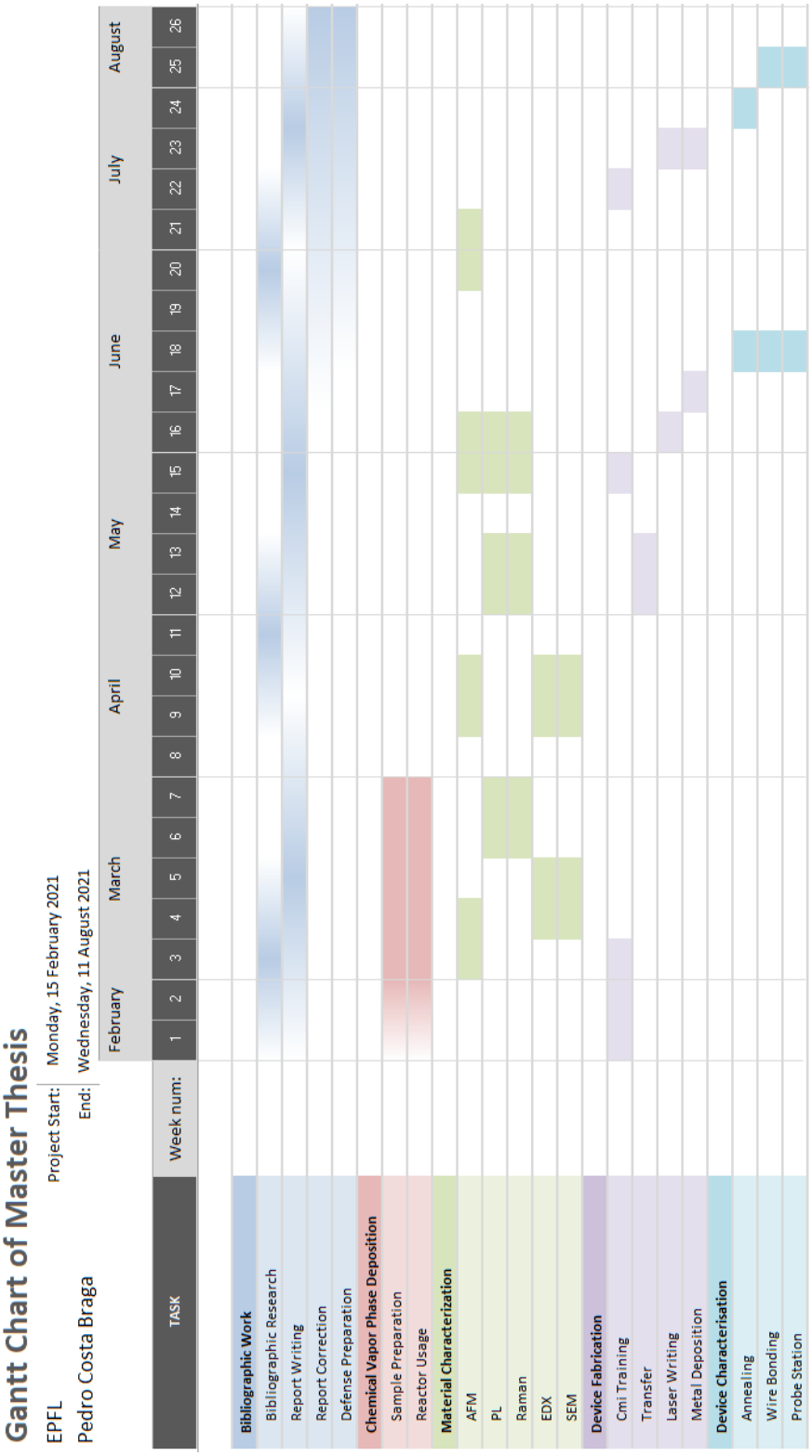

6.2 CMi work flow

Lab : EPFL LANES
Operator Name: **Pedro Costa Braga**
Supervisor Name : Andras Kis
Process Flow Date : 12.03.2021

Phone : +330766723812
Office : BM 2142
E-mail : pedro.costabraga@epfl.ch

CMi EPFL Center of MicroNanoTechnology

☐ Semestral Project ☐ Master Project ☐ Thesis ☐ Other

MoS2 Nanodevices

Description of the fabrication project

Fabrication of suspended **MoS2** devices. **MoS2** is deposited on SiO2 substrates with predefined alignment marks. Individual flakes are contacted using e-beam lithography. Narrow strips are defined using e-beam lithography and negative resist that acts as an etch mask for O2 plasma etching.

Technologies used *!! remove non-used !!*
Mask fabrication, evaporation, positive resist, Lift-off, Dry etching, Wet etching, CPD, E-beam lithography, SEM, EDX

Ebeam litho data - Photolitho masks - Laser direct write data			
Mask #	**Critical Dimension**	**Critical Alignment**	**Remarks**
1	**2 um**	First Mask	Laser writer, Oxide structuration
2	**0.5 um**	100 nm	E-beam lithography, metal contacts
3	**0.5 um**	100 nm	E-beam lithography, etching

Substrate Type
For Device Fabrication: Silicon <100>, Ø100mm, 525um thick, Single Side polished, Prime, p type, 0.1-0.5 Ohm.cm For Material Growth: c-plane Sapphire 102 mm in diameter, 1 mm thick

Interconnections and packaging of final device

Thinning/grinding/polishing of the samples is required at some stage of the process.
☐ No ☐ Yes => confirm involved materials with CMi staff

Dicing of the samples is required at some stage of the process.
☐ No ☐ Yes => confirm dicing layout with CMi staff

Wire-bonding of dies, with glob-top protection, is required at the end of the process.
☐ No ☐ Yes => confirm pads design (size, pitch) and involved materials with CMi staff

Lab : EPFL LANES
Operator Name: **Pedro Costa Braga**
Supervisor Name : Andras Kis
Process Flow Date : 12.03.2021

Phone : +330766723812
Office : BM 2142
E-mail : pedro.costabraga@epfl.ch

CMi EPFL Center of MicroNanoTechnology

Step-by-step process outline

Step	Process description	Cross-section after process
01	**Wet Oxidation** Substrate: *Si, n++* Thickness: cca *0.3 µm*	
02	*Photolithography* MLA150, ACS200, EVG150 Photoresist AZ1512 Sacrificial layer LOR5A 0123 HMDS / NoEBR (topEC) - 1um thick	
03	*Dry Etch* Material : SiO2 Machine: SPTS APS Dielectric Etcher Depth : 150 nm Recipe: SiO2 PR 3:1 Time: 30 s	
04	*Metal evaporation* Material: Cr/Pt Machine: LAB600 **Height:10/50 nm**	
05	*Lift-off* Z1 Plade solvent	
06	*Coating with Photoresist* Serves as protection for dicing. ACS200 Photoresist AZ ECI 3000 0123 HMDS / NoEBR (topEC) - 1um thick	
07	*Dicing* Machine: Disco Saw **Material:**	

08	Wet Stripping of the protective Photoresist layer in Remover 1165 Z2	
09	*O2 plasma cleaning* Machine: Tepla Z11 **Recipe: 06**	
10	*MoS2* *Substrate: c-plane sapphire* **LANES laboratory**	
11	*Characterization (SEM, EDX)* *Materials: MoS2* *Machine: Zeiss LEO 1550, Zeiss MERLIN*	
12	*E-beam litho for strips* Machine: Vistec Material : PMMA	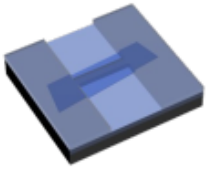
13	*O2/SF6 plasma etching with e-beam resist used as the mask* Machine: Alcatel AMS 200, 20s etch time	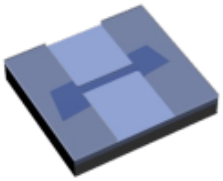
14	*Strip PMMA mask*	
15	*E-beam litho for contacts* Machine: Vistec Material: PMMA/MMA	

Lab : EPFL LANES
Operator Name: **Pedro Costa Braga**
Supervisor Name : Andras Kis
Process Flow Date : 12.03.2021
Phone : +330766723812
Office : BM 2142
E-mail : pedro.costabraga@epfl.ch

CMi EPFL Center of MicroNanoTechnology

16	*Metal evaporation* Machine: Lab600 Material: Ti/Pt, Cr/Pt, Pd, Co/ Au 10+50nm	
17	*Lift-off* Z1 Plade solvent	
18	*Wet Oxide Etch+CPD* Material : SiO2, HF 10% Machine:Wet bench, Tousimis CPD Depth : 100 nm	

Rem. : You can add any interesting information about this process flow, your devices, ...